JETIR.ORG ISSN: 2349-5162 | ESTD Year : 2014 | Monthly Issue
JOURNAL OF EMERGING TECHNOLOGIES AND INNOVATIVE RESEARCH (JETIR)
An International Scholarly Open Access, Peer-reviewed, Refereed Journal

Experimental and theoretical probations of Lacosamide metabolites - Amide and Ester derivative: Chemical synthesis, Characterizations, DFT computations, Optical activity, In Vitro and In Silico ADMET assessment with Molecular docking estimations.

N. Elumalai [a], Magesh Subramaniyan[b], T. Kamatchi[c], C.T. Ravichandran[a*],

[a] Research Department of Chemistry, Arignar Anna Government Arts College, Cheyyar - 604 407, Tamilnadu, India. (Affiliated to Thiruvalluvar University, Vellore – 632 115, Tamilnadu, India.)

[b] PG and Research Department of Chemistry, Thiru.A.Govindasamy Government Arts College, Tindivanam, Villupuram-604 307, Tamilnadu, India.

[c] Department of Physics, Arunai Engineering College (An Autonomous Institution), Velu Nagar, Mathur,Tiruvannamalai-606 603, Tamilnadu, India.

***Corresponding Author**: ctrchem22@gmail.com;

Abstract

Amide derivative LAC002 is distinct form of the compound lacosamide that have been produced efficiently and in substantial amounts. Along with elemental analysis, FT-IR, ^{1}H NMR, and ^{13}C NMR spectroscopy has been used to examine the structures of the molecules. In order to examine the compounds' electrical and structural characteristics, as well as how they pertain to cancer inhibition, DFT (density functional theory) simulations were utilized. Utilizing the 6-311++G(d,p) basis set and the B3LYP calculation method, the optimum structure and vibrational analysis frequency bands were identified. The bonding energies and ellipticity were calculated using the electron localization function. By comparing simulated data with practical outcomes, FT-IR and FT-Raman spectroscopies were employed for generating functional groups of data. While donor-acceptor interactions were investigated using NBO, the molecule's reactive areas were investigated utilizing the ELF, LOL, respectively, along with molecular electrostatic potential (MEP).It is projected to have a much stronger high polarizability (β = 42.963 e.s.u×$\mathbf{10^{-30}}$) than urea (β = 6.537 ×$\mathbf{10^{-30}}$). It is possible to suggest that the LAC002 molecule has better NLO characteristics. The wavelength of highest absorption was identified using UV-Vis spectra in conjunction with the TD DFT technique. The bioavailability score of LAC002 is 0.55, which is a measure of what happens shortly and effectively a medication enters into the body. Additionally, biological investigations are being conducted, including molecular docking and drug-likeness assessments.

Keywords: DFT, NBO, ELF, LOL, MEP, Docking.

1. Introduction

On an international scale, condition epilepsy is thought to be the most commonly observed neurological illnesses, impacting over 50 million individuals across every age category [1–4]. In adults and children aged one month and above who are unable to take oral drugs, lacosamide metabolic by products have been utilized to treat partial onset seizures, or seizures that affect only one area of the brain. To treat primary generalized tonic-clonic attacks (spasms affecting every part of the body) in both adults and kids aged 4 and above who are unable to take oral drugs, lacosamide metabolites are also used in conjunction with various other drugs. A class of medications categorized as anticonvulsants includes lacosamide's derivatives. That heals out of suppressing inappropriate brain nerve impulses. Lacosamide metabolites are produced by therapeutic chemical processes and studied using spectroscopic methods. Patients with brain tumor-related epilepsy could potentially require to undergo polytherapy, which can negatively impact their quality of life, and the condition is frequently treatment resistant to the medication [6].

Cancer is a prevalent condition across people worldwide at at the moment. Recently, there is an immediate need for cancer consciousness, cancer therapy, and the development of novel cancer medications [7,8]. By upcoming years more than 20 million more instances of cancer are expected to occur, according to World Health Organization (WHO) projections [9,10]. The unpredictable development and division in the cells that results in adverse outcomes is referred in the form of illnesses such as cancer [11, 12]. The rise in novel mutagenesis illnesses over the last three decades in particular has driven a need for new medication improvements [13]. Incorporating new medications into clinical studies requires research spanning from clinical toxicity to fundamental pharmaceutical science [14]. New antineoplastic drugs can be developed to lower the number of cancer fatalities due to advances in technology and an increasing awareness of human neoplastic disorders [15–18]. The medications levetiracetam, lacosamide, lamotrigine, oxcarbazepine, and valproic acid have had promising results across various malignancies. Even though antiepileptic therapies could serve as a promising option for supportive therapies for cancer, additional research on their safety and effectiveness in clinical investigations is needed [19].

Lacosamide's metabolites, [(2R)-2-acetamido-3-(benzylamino)-3-oxopropyl] acetate, have a molecular mass of 278.30 g/mol and the chemical composition $C_{14}H_{18}N_2O_4$. According to a review of the literature, the above-named chemical has not yet been the subject of computational along with biological research. Present investigation aims to determine the studied compound's structural, vibrational, electrical, biological, and molecular docking characteristics both experimental and computationally. For evaluating experimental results along with computational vibrating spectra calculations, B3LYP-Density Calculation Functional Methods implements the 6-311++G (d, p) basis set of data. The theoretical energy gap was calculated, and also each of the lowest unoccupied (LUMO) in addition to highest occupied (HOMO) molecular orbitals were investigated. DFT/B3LYP (IEFPCM) is used to evaluate UV visible spectra in a range of solvents and compare with experimental data. During electrical energy stimulation, the energy gap known as HOMO-LUMO is investigated with respect to different band-gap and also bonding energy levels. Multiwave functional evaluation is performed utilizing techniques that include the localized orbital locator (LOL) and the electron localization function (ELF). Finding the density of electrons in various orbitals and the proper stabilizing energy is made easier through the analysis of the natural bond orbitals (NBO). Using two descriptors, reactive sites are examined. The electrostatic potential surface of molecules that are distinct (MEPs) is seen. Quantum chemical analysis is used to explain nonlinear (NLO) optical performance. The biochemical effectiveness is demonstrated by drug similarity, ADME, and toxicity criteria. Anticancer protein sequences are docked, and the lowest possible energy of binding has been achieved.

2. Experimental method:

2.1 Molecular mechanism of Lacosamide's anti-cancer bioactive metabolite

2.1.1 Step-1, Chemical Synthesis of compound (1):

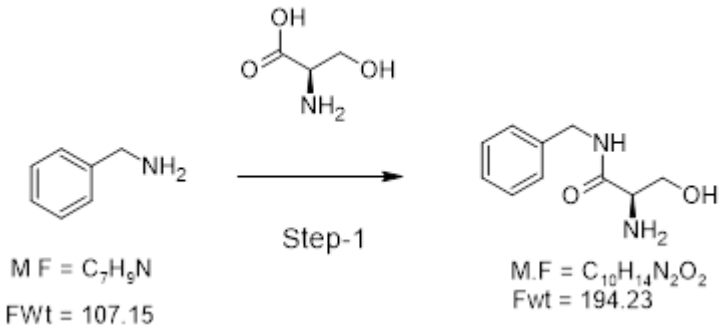


Fig 1. Synthesis mechanism to produce lacosamide.

Experimental procedure:

The chemical, which is also known as benzylamine (0.5g, 1.67mmol), 4-dimethylaminopyridine (0.102g, 0.835mmol), aceticanhydride (2.835ml, 30 mmol), and triethylamine (2.62ml, 18.7mmol), has been agitated for several hours at 95°C in a nitrogen-containing atmosphere. Through the use of 3% methanol in dichloromethane, the reaction was seen using TLC. After the initial material was entirely consumed, TLC in UV was used to identify the expected outcome. Following the chemical process had dropped to room temperature is preferred, 50 ml of the solution of diethyl ether was introduced, then the end product was collected with cleansing through a Celite pad. After being cleaned with three 50 ml batches of water and twenty milliliters of a brine solution the resultant filtrate was allowed to dry using sodium sulfate. The crude product, a brownish solid, was obtained by vacuum evaporating the solvent that was used at 52 degrees Celsius. The unrefined product has been extracted in a dichloromethane solution containing 10% EtOAc. The compound Lacosamide was obtained by means of crystalline formation from the compound methanol (0.8g). The synthesis pathway for lacosamide is shown in Figure 1.

2.1.2 Step-2, Chemical Synthesis of compound LAC002:

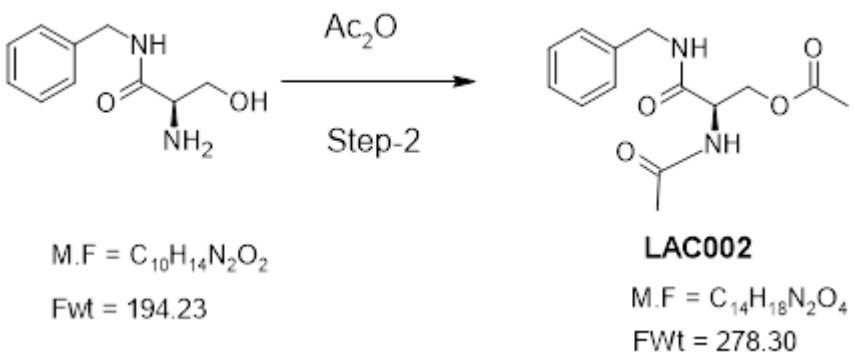


Fig 2. Synthesis mechanism to produce the metabolites of lacosamide.

Experimental procedure:

The chemical compound Lacosamide (0.25g, 0.65mmol) has been dissolved using DCM (2.5ml) at ambient room temperature and then conditioned to 0°C. At 0°C, the AC_2O was gradually added drop by drop, and the resultant mixture underwent stirring for two hours.

TLC was used to evaluate the reaction with 30% ethyl acetate in hexane. The first product vanished, and also a fresh UV area of activity could be observed through the TLC. Five milliliters of the water that is ice cold was incorporated to the mixture in order to extract the chemical solvent. The resulting solution was then completely purified by means of the chemical ethyl acetate (3 x 10 ml).

Following an acidification process together with 15% HCl (PH = 2), an aqueous layer was then separated using ethyl acetate (3x15 ml), cleansed along with brine (5 ml), subsequently dried out onto sodium sulfate. Figure 2 depicts the synthesis method for producing the lacosamide metabolites. Vacuum concentration at 45°C produced a shade of brown a gel-like substance derived from the organic liquid components. Following the use of 20% ethyl acetate in hexane for Pre-TLC purification from the main final product, 0.1g of pure chemical [(2R)-2-acetamido-3-(benzylamino)-3-oxopropyl] acetate was extracted.

3. Specifications of the computation:

By applying the basis set, 6-311++G (d, p) [20,21] and the Gaussian-09 W application technique, the B3LYP density functional was created, which has subsequently been used to determine the fundamental frequencies of vibration as well as the composition of molecular structures. Detailed vibrational frequency assignments were calculated by means of the Chemcraft software [22] incorporating symmetry factors and accessible compounds that were associated. At the DFT/6-311++ G(d,p) level, the geometrical elements of the computational model of LAC002 have initially been optimized with complete relaxation over their potential energy surfaces. The results of these geometrical forms were then utilized as data to perform additional computations at the DFT(B3LYP) levelling was shown in figure 4. The title compound's sites of reaction are visible through the molecular electrostatic potential (MEP). The aforementioned approach was used to explore the global reactivity characteristics and frontier molecular orbitals (FMOs). Additionally, the chosen molecule's theoretical NMR and UV-visible spectra for different solvents were calculated. NBO simulations were utilized to estimate donor- acceptor interactions and stabilizing measures energy values at various levels of B3LYP/6-311++G(d,p) [23].

4. Results and discussion:

4.1. Powder X-ray diffraction analysis

PXRD is a technique that provides an outline which includes precise data on the atomic orientations, lattice specifications, and also structural configuration [24]. The powder X-ray diffraction characteristics of the LC002 compound were assessed using a tool called an X-ray diffractometer (PXRD, a device made by BrukerD8 Advance, Germany). The measuring scanning angle of 2θ varied between the 5° to 60° as a result of with an average stepping in size of 0.009°/2θ approximate 25-30°C by means of a Cu that provides the radiation (2.2-Kilowatt anode made from Cu ceramic radiation tube). The current research investigation includes crystalline form LAC002. The LAC002 polymorphic of Lacosamide might exhibit X- Ray powder diffraction characteristics with peak positions at 3.7, 5.5, 8.2, 10.9, 15.9, 19.6, or 23.7 degrees ± 0.2 degrees of 2-theta, respectively and shown in fig.3.

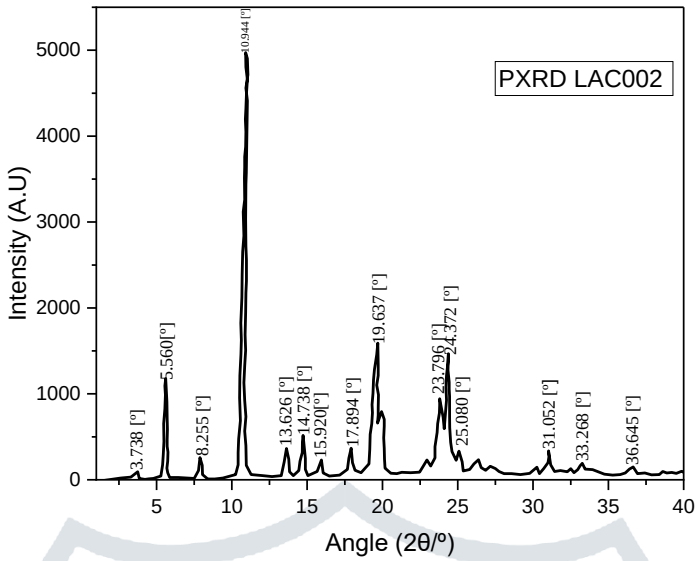


Fig 3. PXRD of LAC002.

4.2. Geometry optimization

Determining the individual atomic locations that provide the structure's the lowest-energy state is how the concept of density functional theory (DFT) determines the molecule's geometrical structure. The procedure, called geometry optimization, entails repeatedly shifting the atoms' locations inside the structure of the molecule until the forces that are acting on atoms are reduced to a low-energy, sustainable form [25]. In order to minimize energy, the molecular composition of LAC002 has been optimized using the DFT recommended basis set indicated previously. Using atom numbering, Fig. 4 shows the optimal shape of the LAC002 molecule, which has 38 atoms and 38 bonds. For the molecule being tested, the optimization produced C1 point group symmetry. In Table 1, some of the most stable structural characteristics of LAC002, such as bond lengths, bond angles, and torsional angles, are compiled. All of the torsional angles fall between 0˚ and 180˚. It is evident from these dihedral angles that the molecule LAC002 is non-planar, as these DFT calculations assumed C1 point group symmetry. For the C1-C13, N2-C4, C3-O1, and C4-H4 bonds, the corresponding estimated bond lengths were 1.545, 1.478, 1.388, and 1.094. Between C1 and C13, the largest intermolecular distances were determined. The bond angles with the greatest values are O4-C13-C14, O1-C13-O4, O3-C11-N1, and C9-C12-C10 (126.5, 122.3, 121.3, 119.6).

Table 1. Optimized LAC002 molecule parameters for structure at B3LYP/6-311++G (d, p).

Parameters Bond length (Å)	**Values B3LYP/6311G++ (d,p)**	**Parameters Bond length (º)**	**Values B3LYP/6311G++ (d,p)**
$H_2 - C_2$	1.0969	$H_{16} - C_{14} - H_{17}$	110.437
$H_7 - N_2$	1.0136	$C_{13} - C_{14} - H_{17}$	109.597
$H_9 - C_8$	1.0890	$O_4 - C_{13} - C_{14}$	126.564
$H_1 - C_1$	1.1005	$O_1 - C_{13} - O_4$	122.333
$O_4 - C_{13}$	1.2408	$C_9 - C_{12} - C_{10}$	119.674
$H_3 - C_2$	1.0929	$N_1 - C_6 - C_{11}$	116.285
$H_{11} - C_{10}$	1.0874	$O_3 - C_6 - N_1$	121.355

$H_5 - C_4$	1.0968	$N_2 - C_4 - H_4$	106.012
$O_3 - C_6$	1.2643	$H_4 - C_4 - H_5$	108.203
$C_2 - C_1$	1.5397	$O_2 - C_3 - C_1$	121.040
$C_2 - O_1$	1.4749	$O_1 - C_2 - H_3$	109.816
$C_8 - C_{10}$	1.4092	$C_3 - N_2 - C_4$	122.439
$C_8 - C_5$	1.4096	$C_3 - N_2 - H_7$	119.399
$N_2 - C_4$	1.4789	**Torsional angles**	
$N_2 - C_3$	1.3680	$H_2 - C_2 - C_1 - H_1$	51.193
$C_{10} - C_{12}$	1.4067	$H_2 - C_2 - C_1 - N_1$	169.98
$C_1 - C_{13}$	1.5458	$H_3 - C_2 - C_1 - C_3$	171.18
$C_1 - N_1$	1.4586	$H_3 - C_2 - O_1 - C_{13}$	69.811
$C_4 - C_5$	1.5243	$H_9 - C_8 - C_{10} - C_{12}$	179.62
$C_4 - H_4$	1.0947	$C_{10} - C_8 - C_5 - C_4$	179.66
$C_{13} - O_1$	1.3883	$H_7 - N_2 - C_4 - H_4$	166.46
$C_{13} - C_{14}$	1.5087	$C_3 - N_2 - C_4 - C_5$	101.48
$C_5 - C_7$	1.4138	$H_7 - N_2 - C_3 - O_2$	175.49
$C_3 - O_2$	1.2608	$H_1 - C_1 - C_3 - O_2$	121.32
$C_6 - N_1$	1.3718	$H_1 - C_1 - N_1 - C_6$	43.964
$C_6 - C_{11}$	1.5202	$C_2 - C_1 - N_1 - H_6$	112.75
$N_1 - H_6$	1.0167	$C_3 - C_1 - N_1 - C_6$	162.23
$C_{12} - H_{15}$	1.0874	$O_1 - C_{13} - C_{14} - H_{17}$	168.11
$C_{12} - C_9$	1.4104	$O_3 - C_6 - N_1 - H_6$	168.11
$H_{17} - C_{14}$	1.0919	$N_1 - C_6 - C_{11} - H_{13}$	125.90

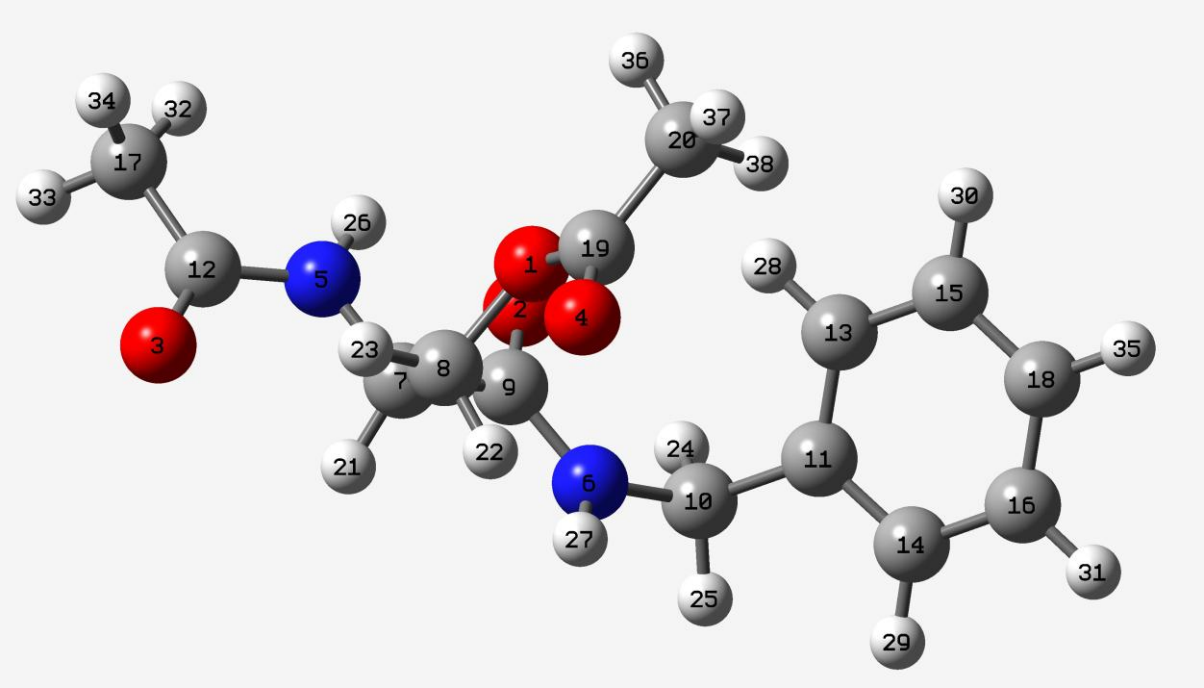


Fig 4. Optimized LAC002 image with appropriate atom numbering beginning at low- energy concentrations.

4.3 HOMO-LUMO study

Integrating the applications of the LUMO (the lowest unoccupied molecular orbital) with the highest occupied molecular orbital (HOMO) allows for the prediction of several characteristics, including the electrostatic charges traits, chemical mixture reactions, biological functions, stabilization, and also reactivity in order of chemical substances [26].

For chemical compounds having LAC002 and other parameters, Density Functional Theory (DFT) provides important information on the molecules' reactivity, stability, and conductive characteristics. The LUMO and HOMO vibrations, which at first refer for the lowest unoccupied together with highest occupied orbitals, correspondingly, have significance for the reliability study. The lowered values of -0.8273 eV (LUMO) and -6.9198 eV (HOMO) in this particular instance suggest that the molecular structure was probably theoretically persistent. The compound's electrical conductivity is shown by its predicted bandgap of 6.0925 eV. It is likely that the compound might have the properties of a semiconductor or an insulator with a large gap. An atom's electronegativity, a measurement of its capacity to draw electrons in the structure has been determined to be 0.8273eV. This positive number indicates that electrons are significantly attracted to it. The chemical potential through which is the amount of potential energy needed to facilitate the molecule's ability to discharge or receive electrons, is -0.3046 eV, demonstrating the compound's propensity to undergo electron-related actions.

The global softness and hardness metrics obtained from the HOMO and LUMO calculations provide details on the polarization potential and the resistance of the molecule, respectively. 3.0462 eV for global hardness and 0.1641 eV for equivalent softness provided insight into the molecule's electrical behavior. The total of the global hardness and chemical potential yields the electrophilicity index, which is 0.0152 eV. A compound's reactivity is measured by the aforementioned index, and higher values imply more reactivity. The DFT simulations highlight the LAC002 molecule displayed in Figure 5, with its intrinsic stability, insulator or semiconductor-like characteristics, electron-attracting configuration, and reactive properties in that pattern.

In a variety of disciplines, such as chemistry and materials science, these discoveries are essential for comprehending the possible uses of substances. Chemical potential, softness, and hardness are some of the DFT's distinct attributes (listed in Table 2), which help us better understand LAC002's molecular properties and point to its possible uses in a variety of sectors.

The following mathematical equations can be used to express particular characteristics of these parameters:

Energy gap = $E_g = E_{LUMO} - E_{HOMO}$ .....(1)

Ionization energy = $I = -E_{HOMO}$ .....(2)

Affinity for electrons = $A = -E_{LUMO}$ .....(3)

Electronic chemical potential = $\mu = \frac{-I+A}{2}$.....(4)

Global hardness = $\eta = \frac{I-A}{2}$.....(5)

Softness =$S = \frac{1}{2\eta}$ .....(6)

Global electrophilicity index = $\omega = \frac{\mu^2}{2\eta}$ .....(7)

Table 2. Global calculated parameters for LAC002

S. No.	Compound id	HOMO eV	LUMO eV	Band gap eV	Electron egativity eV	Chemical potential eV	Global hardness eV	Global softness eV	Electrophilicity index eV
1	LAC002	-6.9198	-0.8273	6.0925	0.8273	-0.3046	3.0462	0.1641	0.0152

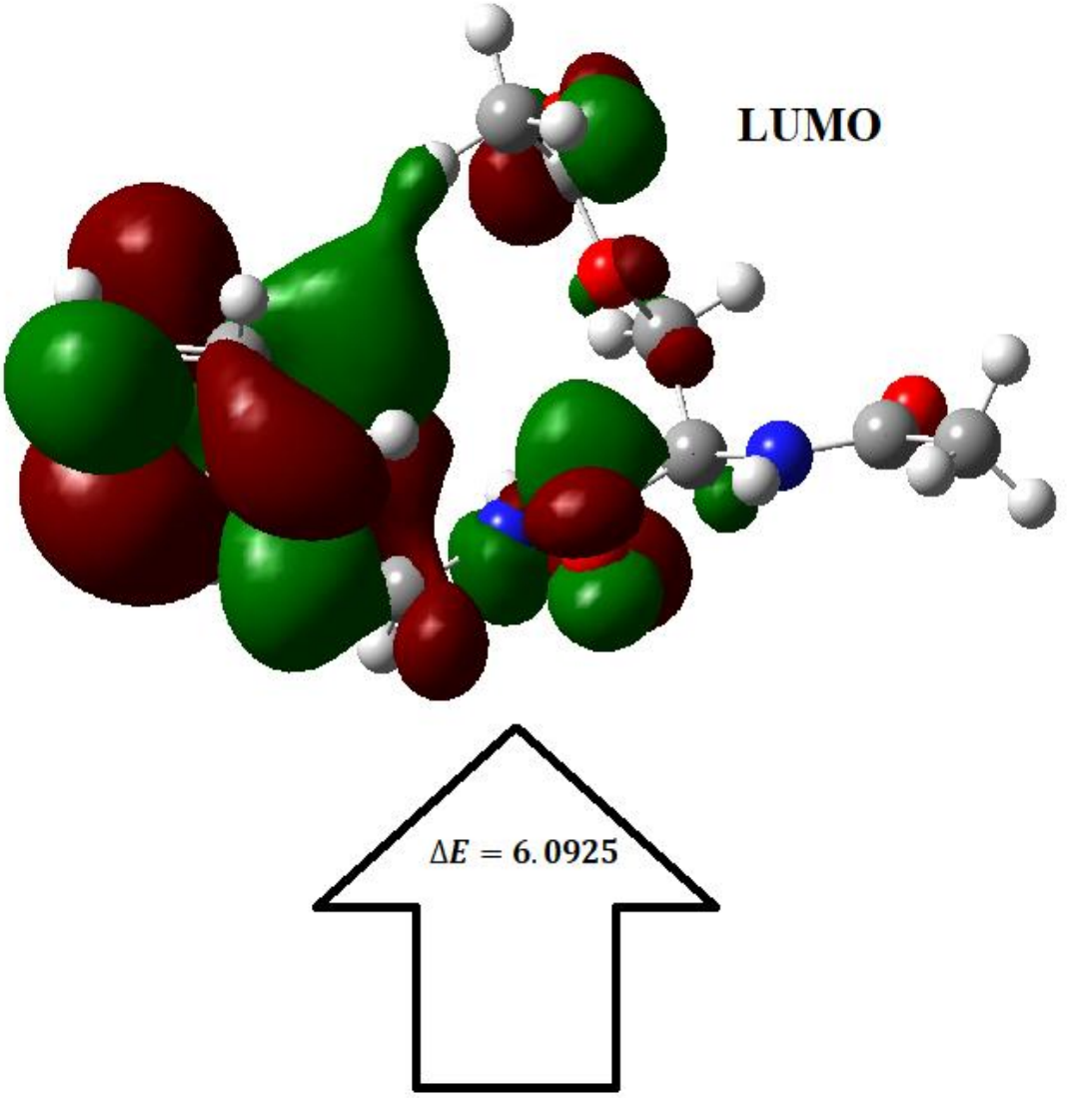

LUMO
$\Delta E = 6.0925$
HOMO

Fig. 5 LAC002's frontier molecular orbitals.

4.4 Mulliken atomic charge

The Mulliken charges, which are used to compute the electrically charged potential of an electronic arrangement following molecular relocation, are intimately related to the vibrational analysis characteristics of the molecules included within it. Consequently, the chemical bonds of the molecule were immediately affected. This affects polarizability, electrical structure, dipole moment, and other properties of the molecular system. According to the Mulliken population assessment, the total net atomic values associated with the LAC002 compound are illustrated in Figs. 6 and 7 that are described in Table 3. The results of the analysis revealed that the opposite potential remained decentralized in the oxygen group of atoms whereas the compound lacked an overall potential. The LAC002 molecule's hydrogen bonding atoms are the least negatively charged. The typical negative charge of nitrogen atoms (N) ranges from -0.635 to -0.661. The corresponding negative charges of oxygen atoms (O) range from -0.387 to -0.476. Atoms of hydrogen (H) typically have positive charges between 0.152 and 0.363. A certain amount of fluctuation in the charged states associated with carbon atoms bonded to one neighboring and to the remaining atoms indicated variations regarding their substance and connect with one another.

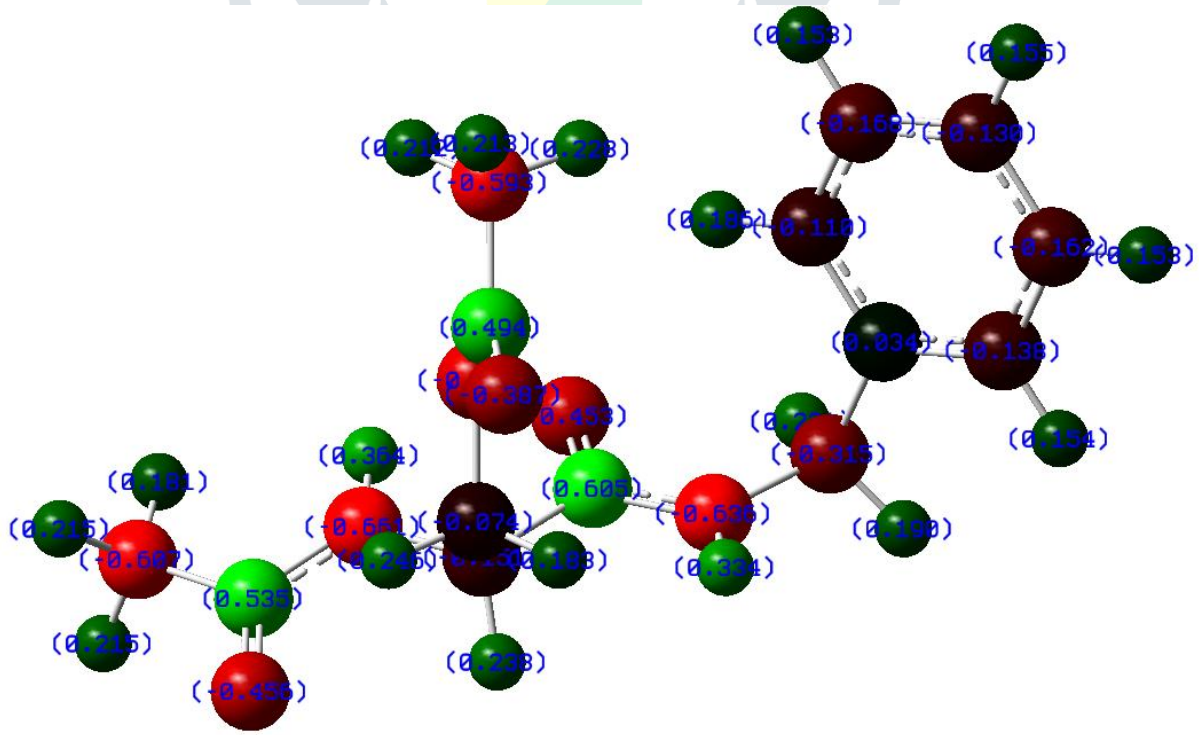


Fig. 6 Mulliken charges distributions of LAC002 structure

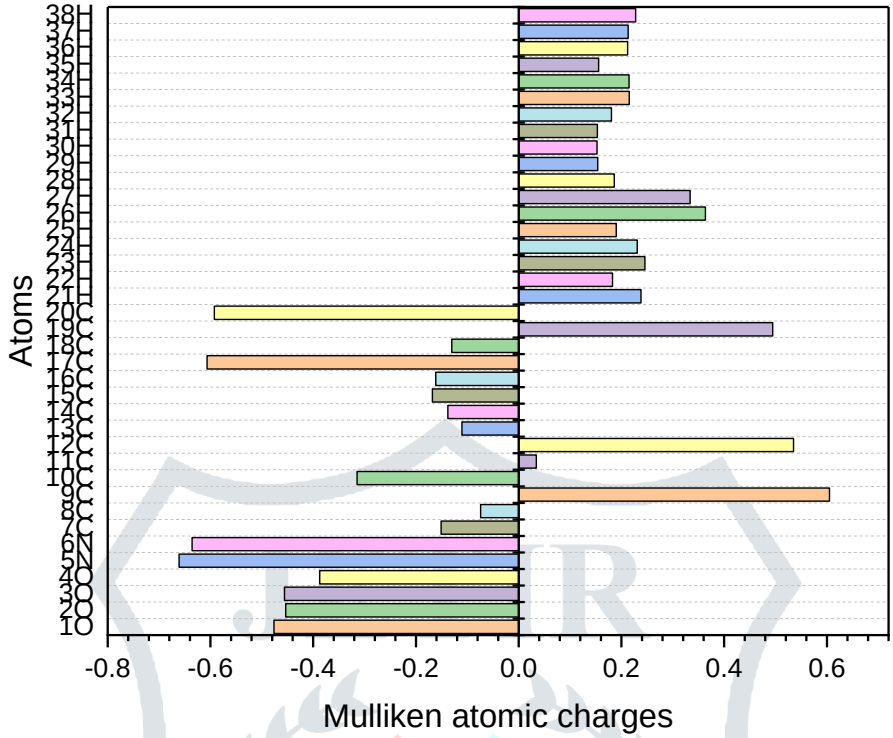


Fig. 7 Mulliken charges of LAC002

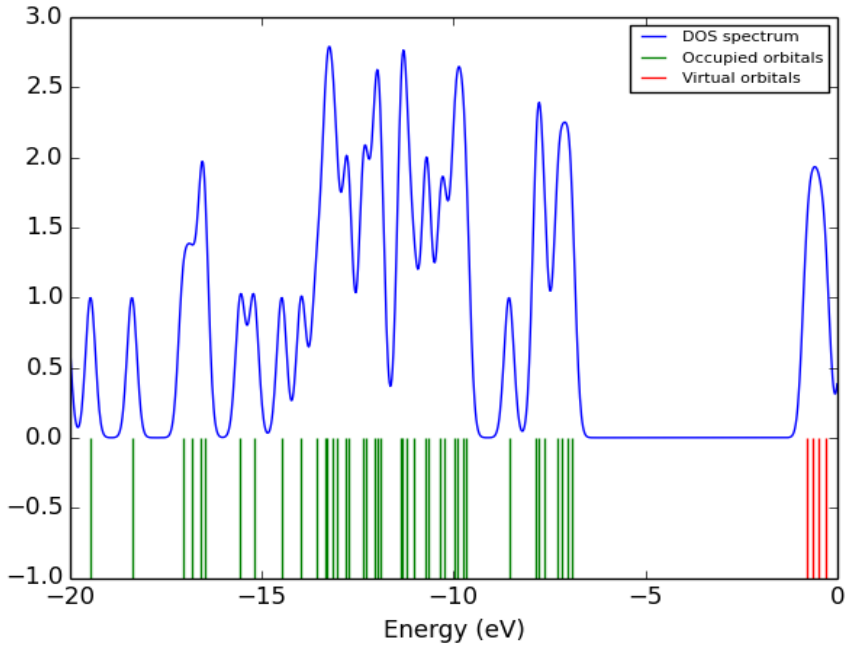
Table 3. Displays the Mulliken charge distribution as calculated upon by B3LYP/6-311++G (d, p) of LAC002.

Atoms	Mulliken Charges	Atoms	Mulliken Charges
1O	-0.476445	20C	-0.592632
2O	-0.453378	21H	0.237895
3O	-0.455796	22H	0.182540
4O	-0.387463	23H	0.245521
5N	-0.661013	24H	0.230928
6N	-0.635832	25H	0.189875
7C	-0.151173	26H	0.363550
8C	-0.074301	27H	0.333839
9C	0.604955	28H	0.186039
10C	-0.314505	29H	0.153919
11C	0.034298	30H	0.152516
12C	0.534910	31H	0.153236
13C	-0.110405	32H	0.180602
14C	-0.137950	33H	0.215039

15C	-0.168172	34H	0.214900
16C	-0.161511	35H	0.155484
17C	-0.606834	36H	0.212218
18C	-0.130141	37H	0.213057
19C	0.494433	38H	0.227797

4.5 Total DOS spectrum

The energy levels in the boundary area may be quasi-degenerate for adjacent orbitals. When this happens, using the HOMO and LUMO alone to describe the boundaries of orbitals could not be realistic. The DOS [27,28] states based on Mulliken populations study were therefore computed and created by combining the Gauss contours about a unit height with FWHM about 0.3 eV with molecular orbital data and the GaussSum2.2 software [29]. In Figure 8, the plotted DOS of LAC002 is displayed. The main purpose behind this Density of States picture intended to demonstrate the manner in which the MOS particles' positive and negative charges respectively assist in chemical-based interactions. In their ground states, anions and cations are fundamentally shown visually as neutral atoms [30].



(a)

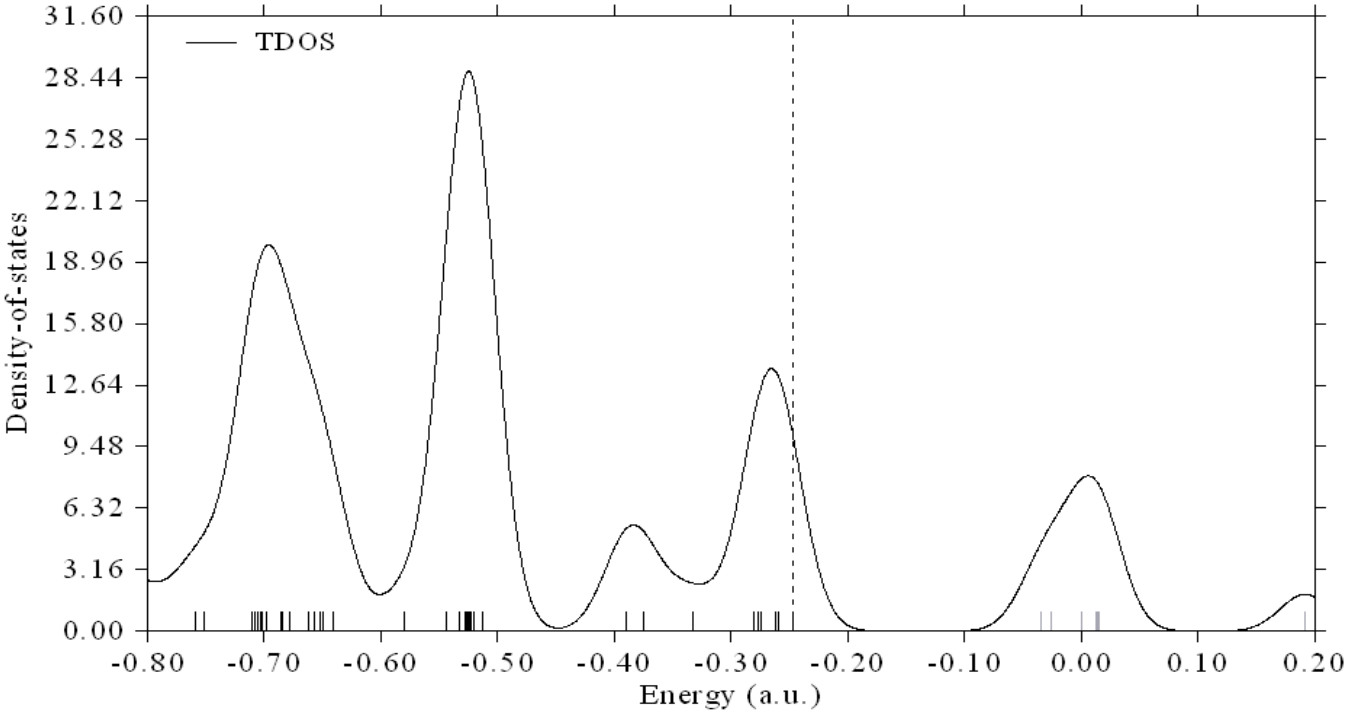


Fig. 8. The LAC002 estimated the TDOS diagram

4.6 Molecular electrostatic potentials (MEPS)

The locations on biological molecules whereby chemicals responded have been identified by utilizing measurements of molecule-level electrostatic fields potential. The shade of blue utilized in the above graphic represents the highest possible positive in order potential, then whereas the color bright red denotes the highest possible negative in value potential. When it comes to identifying the precise molecular areas that play a major role in the biological activity, this visualization is very helpful [31]. The predicted chemical structure's molecular electrostatic potential is seen in three dimensions in Figure 8. The red within the color map indicates overall negatively charged zone, while the electron's population is bigger, while blue

indicates the positively charged region, within which the total number of electrons is smaller. The neutral charges of the electrostatic potential were shown by an appearance of green [32]. LAC002's negative and positive regions range from $-6.660e^{-2}$ to $+6.660e^{-2}$a.u .The zones of LAC002 that are positive and negative vary from the bright red complexion in this chemical combination indicates that there is more negativity surrounding the oxygen atoms. It was also a little negative close to the oxygen molecules. The remaining molecules, including those that contain nitrogen, are represented by the blue-green coloration of the strongly nucleophilic in region that follows.Because of the interactions that occur between the proton and electron, it is simple to determine that the molecule configuration is photonic by identifying its reactive components.

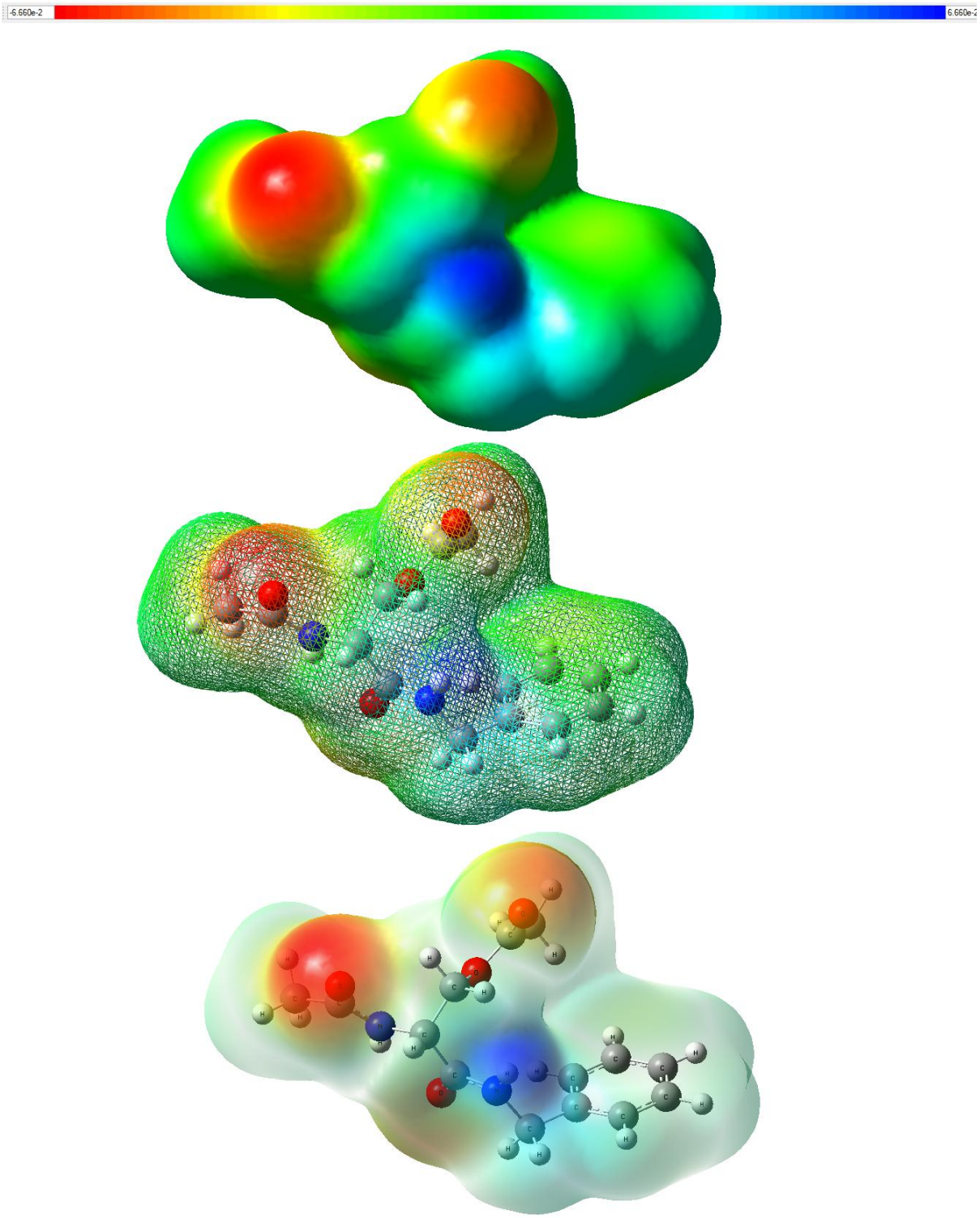


Fig. 8 a) Solid view b) Mesh view c) Transparent view MEP of LAC002

4.7 ELF and LOL analysis

Making use of LOL mappings and electron localization function visualizations, surface profiling based on the covalent bond has been done. The electric charge surrounds of every atom were illustrated using an outline containing a wide or narrow area. The aforementioned enables the discovery of a pair of electrons over a surface of the molecule [33]. The chemical conflict between LOL and ELF is comparable since both are determined by the kinetic energy density. ELF as a on the alternative hand, results from the electron pair density that existed.

The LOL method is utilized whenever localized orbitals overlapping but only indicates the color gradient between the localized orbitals [34,35]. The contoured maps as well as colour shaded visualize of the hydrogen-bonded region are shown in Figure 9(a) and contain the ELF and LOL images of the chosen molecule. Although the ELF map is designed to be in the 0.0-1.0 range, the electrons that were delocalized are positioned in the reduced range (0.5). The elevated value suggests that a nuclear layer or covalent link is present in that region, creating a significant position of electrons.Figure 9(a) shows enhanced ELF zones indicating highly concentrated bond and also non-bond electrons surrounding the atoms of hydrogen.

Blue spots depict the delocalized cloud of electrons surrounding particular molecules of carbon (C9, C11, and C13). The ELF map clearly demonstrates the critical spots and their respective positions trajectory, bonds of molecules, and chemically significant regions (both red and orange). The region of electrical depletion separating the inner and also valence surfaces can be observed by the blue circle that surrounds the nitrogen atom N2. The hydrogen atom's core is white in Figure (b), which suggests the electron density is higher than the color scale's top limit of 0.80. Compared to ELF, LOL communicates a lot more intensity and resolution.

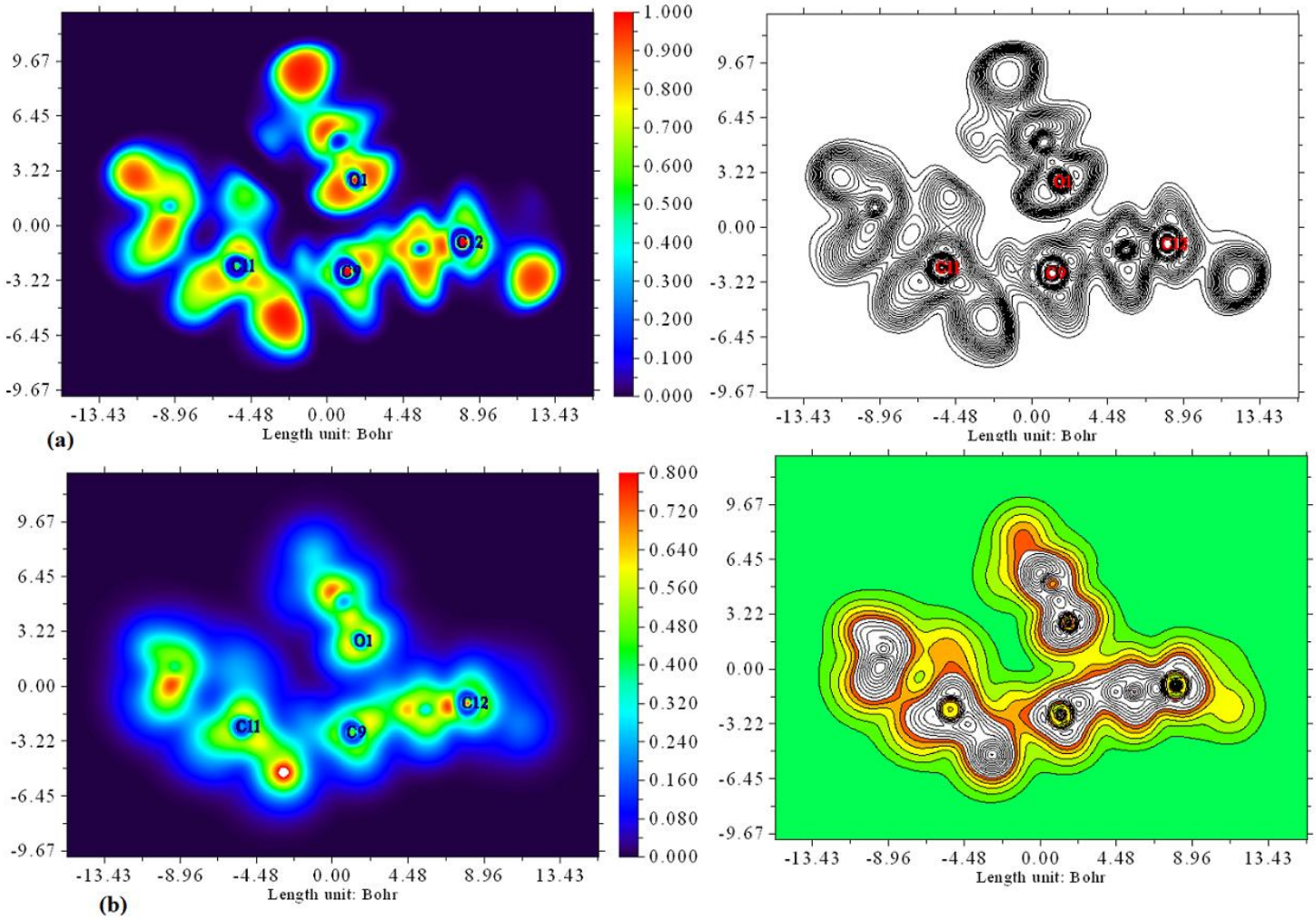


Fig. 9 (a) Color-filled and contour-mapped electron localization function (ELF) maps. (b) Localized orbital locator (LOL) maps with contours and color filled.

4.8 NBO analysis

Natural bond orbital (NBO) analysis is a very effective method for analyzing both intra and intermolecular binding and bond interaction, in addition to offering an excellent basis for researching charge transfer and conjugative interactions in the molecular structure of compounds [36]. The one-dimensional reduced density matrix (1D-RDM) serves as a key representation of the eigen (natural and intrinsic) characteristics associated with the interactions within elements used in NBO analysis [37]. As a result, NBO theory works with the formerly provided energy and structural details. DFT level computation was used to explore the multiple second-order interaction that exist between the fully saturated orbital spaces of one sub system and the unoccupied orbital spaces of another subsystem that may be a symptom of the delocalization or as hyperconjugation [38].

To calculate the stabilization potential, utilize the second-order perturbation formula.

$$E_2 = \Delta E_{ij} = \frac{q_i (F_{ij})^2}{E_i - E_j}$$

where F_{ij} stands for Fock matrix elements, E_i and E_j for diagonal elements, and qi for donor orbital occupancy. The NBO assessment was carried out on the molecules being studied at the DFT (B3LYP)/6-311 G (d, p) level to get a better understanding of the hybridization event, intramolecular interaction, and

dislocation of the concentration of electrons within the arrangement of the molecule. The computed energy parameters for the interaction between the populated i and unoccupied j for the LAC002 molecule are given in Table 4.

Table 4: A summary of the Fock matrix in the NBO basis of the LAC002 molecule using second-order perturbation theory.

Donor NBO (i)	Type	Acceptor NBO (j)	Type	E(2) kcal/mol	E(j)-E(i) a.u.	F(i,j) a.u.
N6	LP (1)	O2-C9	π^*	70.11	0.25	0.119
N5	LP (1)	O3-C12	π^*	64.25	0.26	0.116
O4	LP (2)	O1-C19	σ^*	33.64	0.55	0.123
C13-C15	π	C11-C14	π^*	20.82	0.27	0.068
O2	LP (2)	C7-C9	σ^*	17.91	0.59	0.093
O4	LP (1)	C19	RY*(1)	15.7	1.45	0.135
C20-H38	σ	O4-C19	π^*	6.66	0.49	0.054
C17-H34	σ	O3-C12	π^*	5.02	0.51	0.049
C11-C14	π	N6-C10	σ^*	4.76	0.55	0.05
C12-C17	π	N5-C7	π^*	4.72	0.97	0.061
C13-H28	σ	C11-C14	σ^*	4.65	1.06	0.063
O3-C12	σ^*	O3-C12	π^*	3.73	0.48	0.093
C7-C9	σ	N5-C12	σ^*	3.08	1.09	0.052
C11-C14	π^*	C14	RY*(3)	2.28	0.51	0.073
O2-C9	π^*	O2-C9	σ^*	2.27	0.49	0.073
C11-C14	π^*	N6-C10	σ^*	2.21	0.28	0.051
O2-C9	π	O2-C9	π^*	1.49	0.36	0.023
O4-C19	π	O4-C19	π^*	0.85	0.36	0.016
O1-C19	σ^*	C19	RY*(3)	0.6	0.68	0.075
C10-C11	σ	C10-H25	σ^*	0.57	1	0.021
C13-C15	π	C11	RY*(3)	0.5	0.96	0.021

* (Intermolecular threshold: 0.05 kcal/mol)

4.9 NLO properties

Researchers may review the NLO qualities by examining the structure-activity relationship of molecules, which is made possible by computational calculations. In a chemical complex, a greater NLO responsiveness requires greater molecular polarizability, first-order hyperpolarizability, and an increasing dipole moment. Table 5 displays the computed polarizability (α) and their hyperpolarizability (β) within electrostatic units are subject to investigation derived from the nonlinear optics (NLO) technique. A significant hyperpolarizability (β) value is linked to the nonlinear optical function because of the intramolecular Charge- bonded structure formed by electrons cloud movement from groups that provide electrons [39,40]. The predicted high polarizability (β =**42.963 e.s.u**$\times 10^{-30}$) is several times as potent as urea (β = 6.537 × 10^{-30}). Thus, it may be concluded that the LAC002 molecule has superior NLO characteristics.

Table 5. The outcomes about first order hyperpolarizability(β), polarizability (α), and Dipole moment (μ) of LAC002.

Parameters	LAC002
	S.I (a.u)
μ_x	-1.3161
μ_y	-0.4627
μ_z	0.5420
μ_D	1.4965
α_{xx}	211.54
α_{xy}	-17.365
α_{yy}	148.51
α_{xz}	12.536
α_{yz}	12.859
α_{zz}	154.79
α_{total}	171.59
Δ_α	166.7940
Δ_α	24.71 e.s.u$\times 10^{-24}$
β_{xxx}	129.59
β_{xxy}	33.920
β_{xyy}	-13.036
β_{yyy}	65.590
β_{xxz}	7.010
β_{xyz}	24.506
β_{yyz}	-21.080
β_{xzz}	-8.421
β_{yzz}	-43.260
β_{zzz}	22.693
β_{total}	28.990
$\boldsymbol{\beta_{total}}$	**42.963 e.s.u$\times 10^{-30}$**

4.10. The study of vibrations

A Fourier transform infrared spectrum analyzer (FT-IR), manufactured by Shimadzu, Japanese manufacturer owned by Thermo Fisher Scientific, USA, was used in recording infrared spectra. The wavelengths in the observational measurement range were 400 cm^{-1} to 4000 cm^{-1}. Information on the provided material's transmittance has been identified. The FT-IR spectrum have been provided in the figure 10. The amide group's C=O and N-H stretching peaks were seen in LAC002 around 1649 cm^{-1}. and also 3215 cm^{-1}., respectively. It suggested the ester groups' C=O stretchi
ng band at 1780 cm^{-1}.. When compared to lacosamide, the synthesized combinations had no evidence of any additional peak forms. In the composition with a substantial LCM (Lacosamide) concentration, the C=O peak regarding LC002 became more intense [41]. Similar to LCM (Lacosamide), bonds of hydrogen were found in LC002 combination with donor and acceptor combinations [42]. Even so, the produced preparation LAC002 did not show any notable change or increase in bonding.

The total quantity, excluding the three transversal and rotational degrees of freedom, considering potentially recognizable fundamental non-linear compounds containing the atom of N is the number of seems equivalent to (3N-6). The investigated structure includes 38 atoms and vibrates in 108 distinct modes of representation, which were created using the DFT/B3LYP function. In order to account for full basis set defects and get evacuate of vibrational discord, we scaled up the frequency ranges. Along with calculated IR and also Raman intensity levels accompanying PED components, the following table provides details regarding the exact spectra assignments for the major components. The potential energy distribution (PED) has been applied to provide representations of the typical modes of vibrations using the VEDA tool. Figs. 11 and 12 show the anticipated spectrum for physical evaluation. The PED, which is effective both quantitative as well as qualitative examinations, was used for assigning vibrational spectra.

Table 6 FT-IR parameters for LAC002

The potential energy distribution (PED) calculation-based vibrational assignments.

S.No.	Wave number (cm^{-1})					Vibrational assignments with PED(%)
	Calculated	Observed	Scaled	IR	Raman intensity	
1	3992	3548	3073.81	5	26	ν NH (99)
2	3984	3215	3069.31	6	27	ν NH (100)
3	3976	3061	3063.85	13	28	ν CH (91)
4	3968	-	3058.78	14	29	ν CH (93)
5	3960	-	3055.13	15	30	ν CH (90)
6	3952	-	3004.55	16	31	ν CH (80)
7	3944	-	2997.91	18	35	ν CH (41)
8	3936	-	2996.3	7	21	ν CH (96)
9	3928	-	2988.69	8	22	ν CH (15)

10	3920	2948	2969.58	8	23	ν CH (84)
11	3912	1660	1653.13	10	24	ν CH (78)
12	3904	1649	1632.12	10	25	ν CH (21)
13	3896	-	1613.17	17	32	ν CH (57)
14	3888	-	1602.08	17	33	ν CH (39)
15	3880	-	1593.12	17	34	ν CH (61)
16	3872	-	1560.88	20	36	ν CH (21)
17	3864	-	1549.65	20	37	ν CH (75)
18	3856	-	1536.35	20	38	ν CH (42)
19	3848	-	1530.36	4	19	ν OC (79)
20	3840	-	1522.46	2	9	ν OC (40)
21	3832	-	1519.57	3	12	ν OC (14)
22	3824	1516	1517.69	11	14	ν CC (20)
23	3816	-	1514.15	13	15	ν CC (29)
24	3808	-	1513.37	14	16	ν CC (16)
25	3800	-	1489.73	15	18	ν CC (13)
26	3792	-	1451.01	16	18	ν CC (26)
27	3784	-	1448.6	5	12	ν NC (23)
28	3776	-	1421.58	6	9	ν NC (40)
29	3768	-	1414.27	1	19	ν OC (59)
30	3760	1394	1393.02	20	19	ν CC (59)
31	3752	-	1385.51	5	7	ν NC (49)
32	3744	-	1332.4	10	11	ν CC (50)
33	3736	-	1322.48	17	12	ν CC (43)
34	3728	-	1294.23	6	10	ν NC (46)
35	3720	-	1270.51	8	7	ν CC (31)
36	3712	-	1257.91	7	9	ν CC (20)
37	3704	-	1247.46	1	8	ν OC (45)
38	3696	-	1232.55	11	14	β CCC (19)
39	3688	-	1225.42	26	5	β HNC (43)
40	3680	-	1215.27	27	6	β HNC (22)
41	3672	-	1202.32	28	13	β HCC (29)
42	3664	-	1171.5	29	14	β HCC (30)
43	3656	-	1110.13	30	15	β HCC (27)
44	3648	-	1106.13	31	16	β HCC (26)
45	3640	-	1104.04	35	18	β HCC (39)
46	3632	-	1081.86	21	7	β HCN (59)
47	3624	1064	1053.49	22	8	β HCO (32)
48	3616	-	1050.46	23	8	β HCH (74)
49	3608	-	1046.42	24	10	β HCN (38)
50	3600	-	1044.87	25	10	β HCH (21)
51	3592	-	1034.81	32	17	β HCH (65)
52	3584	-	1023.33	33	17	β HCH (62)
53	3576	-	1011.28	34	17	β HCH (64)
54	3568	-	1002.18	36	20	β HCH (78)

55	3560	-	987.72	37	20	β HCH (57)
56	3552	-	972.94	38	20	β HCH (49)
57	3544	-	969.03	4	19	β OCC (43)
58	3536	-	912.23	2	9	β OCN (15)
59	3528	-	902.17	3	12	β OCC (43)
60	3520	-	896.15	13	15	β CCC (51)
61	3512	-	844.02	14	16	β CCC (51)
62	3504	832	830.21	16	18	β CCC (21)
63	3496	-	792.44	12	5	β CNC (43)
64	3488	-	765.31	9	6	β CNC (26)
65	3480	-	745.28	19	1	β COC (37)
66	3472	-	724.73	20	19	β CCO (42)
67	3464	-	681.73	5	7	β NCC (43)
68	3456	-	658.49	10	11	β CCC (46)
69	3448	-	650.17	17	12	β CCN (26)
70	3440	-	642.52	6	10	β NCC (13)
71	3432	-	628.24	8	7	β CCC (43)
72	3424	-	612.27	7	9	β CCN (24)
73	3416	-	606.45	1	8	β OCC (22)
74	3408	-	594.31	26	5	γ HNCC (86)
75	3400	-	548.71	27	6	γ HNCC (82)
76	3392	512	523.74	28	13	γ HCCC (59)
77	3384	-	493.44	29	14	γ HCCC (24)
78	3376	-	441.87	30	15	γ HCCC (37)
79	3368	428	423.49	31	16	γ HCCC (63)
80	3360	-	417.23	35	18	γ HCCC (68)
81	3352	-	362.03	21	7	γ HCCN (59)
82	3344	-	340.99	22	8	γ HCOC (24)
83	3336	301	300.51	23	8	γ HCOC (37)
84	3328	-	263.05	24	10	γ HCCC (25)
85	3320	-	242.36	25	10	γ HCCC (47)
86	3312	-	233.66	32	17	γ HCCN (60)
87	3304	-	223.86	33	17	γ HCCN (30)
88	3296	-	221.97	34	17	γ HCCN (25)
89	3288	-	205.93	36	20	γ HCCO (40)
90	3280	-	186.76	37	20	γ HCCO (73)
91	3272	-	159.9	38	20	γ HCCO (46)
92	3264	137	128.65	11	14	γ CCCC (36)
93	3256	-	117.92	13	15	γ CCCC (61)
94	3248	-	108.18	14	16	γ CCCC (64)
95	3240	-	103.91	12	5	γ CNCC (69)
96	3232	-	98.32	9	6	γ CNCC (72)
97	3224	-	91.45	19	1	γ COCC (68)
98	3216	-	74.03	20	19	γ CCOC (57)
99	3208	-	56.96	17	12	γ CCNC (54)
100	3200	-	54.25	6	10	γ NCCC (62)
101	3192	-	39.84	8	7	γ CCCN (32)
102	3184	-	3073.81	7	9	γ CCNC (52)

103	3176	-	3069.31	1	8	γ OCCC (50)
104	3168	-	3063.85	2	7	ρ OCNC (41)
105	3160	-	3058.78	4	20	ρ OCOC (76)
106	3152	-	3055.13	12	5	ρ OCNC (72)
107	3144	-	3004.55	9	6	ρ NCCC (10)
108	3136	-	2997.91	19	1	ρ CCCC (41)

[a] stretching; β- bending; ρ -out torsion; γ - torsion;

[b] scaling factor: 0.019 for B3LYP/6-311G (d, p).

[c] Relative intensities are normalizing with the highest peak equal to 100.

[d] Relative Raman intensities normalized to 100.

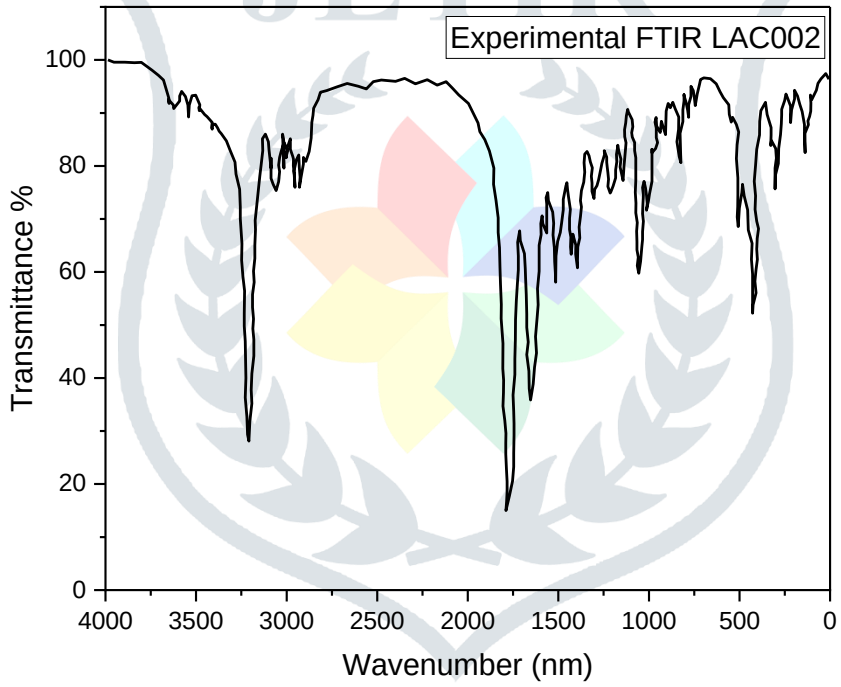


Fig 10. Experimental FTIR spectra of LAC002

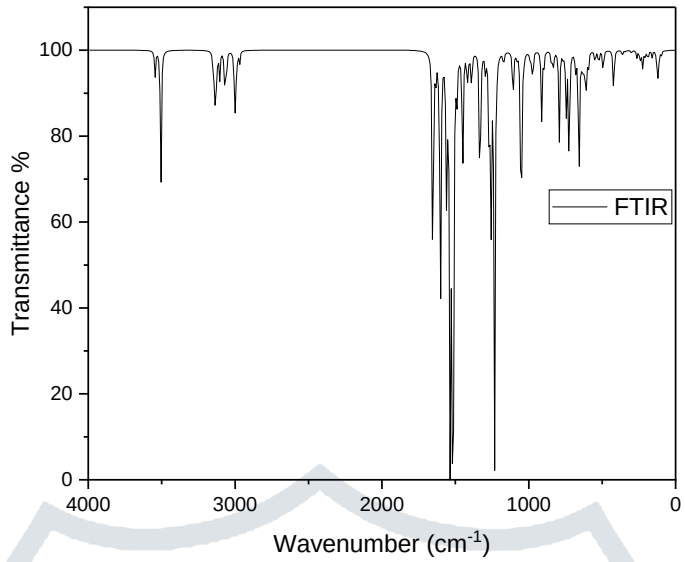


Fig 11. Computational FTIR spectra of LAC002

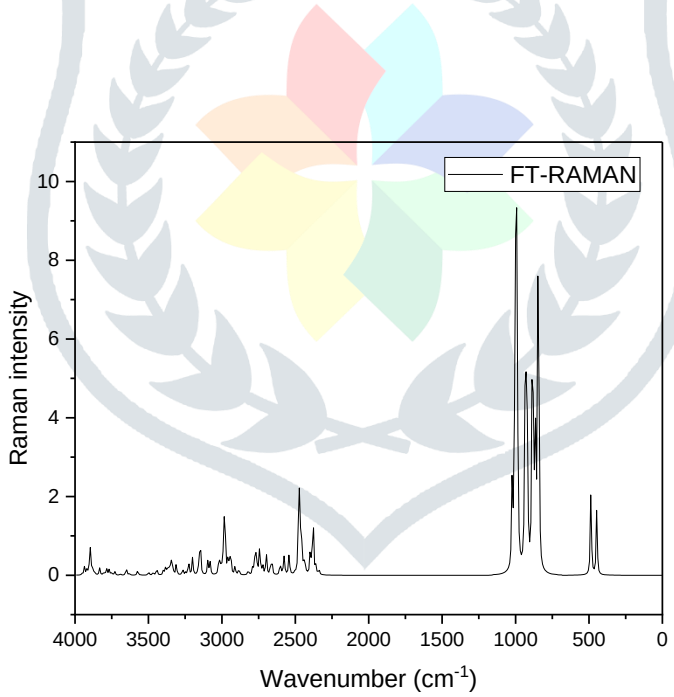


Fig 12. FT-RAMAN spectra of LAC002

4.10. UV-VIS analysis

Lacosamide's UV-Visible (UV-Vis) spectrum fluctuates greatly based on the analytical technique together with chemical solvent utilized. Because the chemical lacks prolonged conjugated dual bond mechanisms, it absorbs very little or insufficient UV radiation hence is unable to absorb the light that is visible [43]. The UV-vis evaluations have been done using a PerkinElmer double beam UV-vis-NIR spectrometer a Jasco V-570 UV-Vis-NIR spectrophotometer model. The spectrum of absorption has been recorded using the absorbance mode with wavelengths that vary from 190 to 1100 nm. Methods of validation has been carried out at room temperature for simplicity. Using the UV absorption spectrum, essential optical traits were acquired. According to the current study, LAC002 absorbs UV light most efficiently at its peak wavelength of 227 nm was shown in fig 13. When compared to previous studies on lacosamide [44,45], this particular wavelength is more sensitive as well as precise for determining its level of concentration.

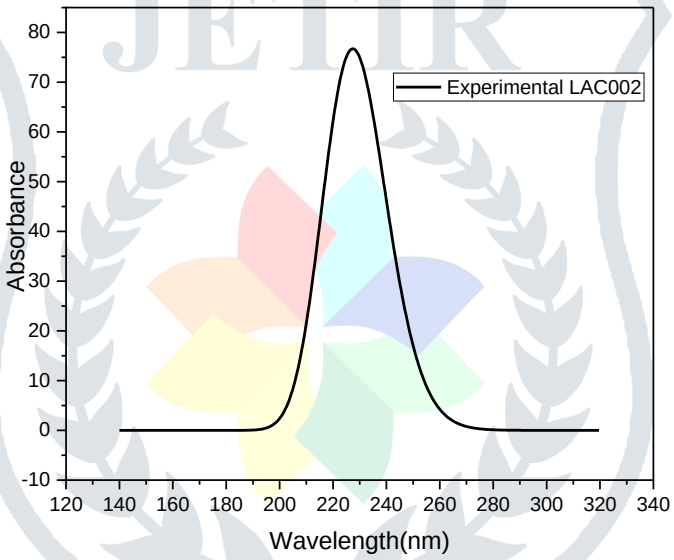


Fig 13. The Experimental UV-visible spectra of LAC002

A theoretical analysis of the specified molecule's UV-visible spectrum was conducted using DMSO, Water, Ethanol, Methanol and Acetone as solvents at the TD-DFT/B3LYP/6-311 ++ G (d, p) level of theory [46–48]. Figure 14 reports the theoretical UV-visible spectra that were derived from Gauss-sum. Figure shows that the wavelength of the greatest absorption is 225,230,235 nm in the order respectively.

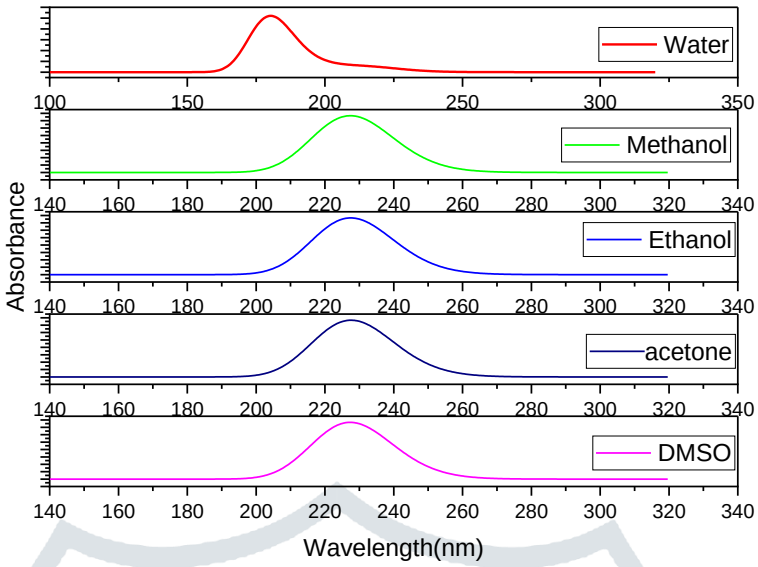


Fig 14. The theoretical UV-visible spectra of LAC002 using various solvents

Because of its polarity, the molecule is able to breakdown polar materials and discriminate charges on ions due to its high dielectric constant and ionic dissolution. When an atom or molecule transitions between its various energies, the oscillator strength—a dimensionless spectroscopic parameter—describes the likelihood that electromagnetic radiation will be absorbed or released. We are already aware of how an absorption molecule's charge distribution is altered by electronic transitions. This suggests that the solvents-solute interactions, which depends on the solvent that is used polarization and transition type, impact the electrical properties of both the grounded and excited forms of the light-absorbing molecule. The interaction that occurs in between a solvent that is present and a solute that is dissolved is known as the process of solvation;when water is involved, solvation is sometimes referred to as hydration. The polarity of the solvent is the most important factor in determining how efficiently it solvates a particular solute. An evaluation of the atomic shift of the studied material follows from this. Chemical composition and absorption go hand in hand. As a material's concentration rises, so does its transmittance. Water exhibits the greatest results out of all of them, and we may use the previous attribute to gauge how strongly other solvents are absorbed. Since they lack the ability to absorb light having wavelength longer than 200 nm, ethanol, water, methanol in order and DMSO are frequently utilized as fluids in a variety of research applications.

4.11. NMR analysis

A Bruker Model 600 MHz analyzer was used for recording the 1H and 13C NMR spectral data. The chemical shift data gathered from the internal standard tetramethylsilane has been provided in δ (ppm). Figures 15 and 16 demonstrate those quantities. 1H NMR (600 MHz, DMSO-d6) δ 8.60 (t, J = 6.1 Hz, 1H), 8.23 (d, J = 8.1 Hz, 1H), 7.34 - 7.20 (m, 5H), 4.56 (dt, J = 8.1, 5.7 Hz, 1H), 4.36 - 4.23 (m, 2H), 4.18 - 4.13 (m, 2H), 1.97 (s, 3H), 1.88 (s, 3H). 13C-NMR (100 MHz, DMSO): δ 170.55, 170.05, 169.37, 139.68, 128.69 (2×C), 127.45 (2×C), 127.20, 64.07, 52.07, 42.53, 23.01, and 21.09.

In research on drugs, NMR (Nuclear Magnetic Resonance) spectrum analysis has been utilized to ascertain three-dimensional structures of protein molecules, find possible potential drugs (leads), verify targets by examining ligand- targets interactions and enhance initial compounds by means of structural-activity relationship (SAR) examination, and even investigate patient reactions to drugs and metabolic processes. It is an adaptable tool for several phases of medical product synthesis, from preliminary screening to in-cell research, due to its capacity to offer atom-level continuously changing data, screened over a variety of biological targets irrespective of needing to prepare for functional assays, and assess interactions

that are weak. A chemical shift of 1.88 ppm is typically observed for a proton on a terminal alkyne group (H-C≡C-) in a ^{1}H Nuclear Magnetic Resonance (NMR) spectrum confirms the metabolite derivation of LCM [49]. It has significant shift in structure can be observed in the estimated ^{13} C NMR spectra for LAC002.

Figure 17 and 18 display the hydrogen, carbon NMR measurements of the LAC002, which was computed using DMSO d6 as the solvent and TMS as that of a source for internal reference When combined with the GIAO approach for computational modelling, NMR provides a powerful tool for predicting and interpreting the structure of large complex biomolecules. According to Table 7, the LAC002 had been investigated through theory as well as experiment for ^{1}H and ^{13}C NMR studies with their assignments in comparison with LCM.

Table 7: Observed and calculated ^{1}H,^{13}C chemical shifts for LAC002 in DMSO-d6 solvent in comparison with LCM.

ATOMS	Experimental shift of LCM (ppm)[50,51]	Experimental shift of LAC002(ppm)	Computational shift of LAC002 (ppm)	Assignment
28-H	7.34 - 7.20	7.34 - 7.20	7.6856	The benzyl phenyl group's aromatic protons.
23-H	4.56	4.56	4.585	Aliphatic C-H proton ions near the both amide groups
22-H	4.18–4.13	4.18 - 4.13	4.1497	Methoxy-substituted C-H protons
33-H	1.97	1.97	2.0185	Acetamide methyl group
32-H	-	1.88	1.7817	alkyne group (H-C≡C-)
9-C	171.98	170.55	176.0567	C=O (Amide)
11-C	169.73	169.37	-	C=O (Acetamido)
17-C	23	23.01	29.3582	Acetamide methyl carbon
20-C	-	21.09.	27.6314	a methyl group (C=O)

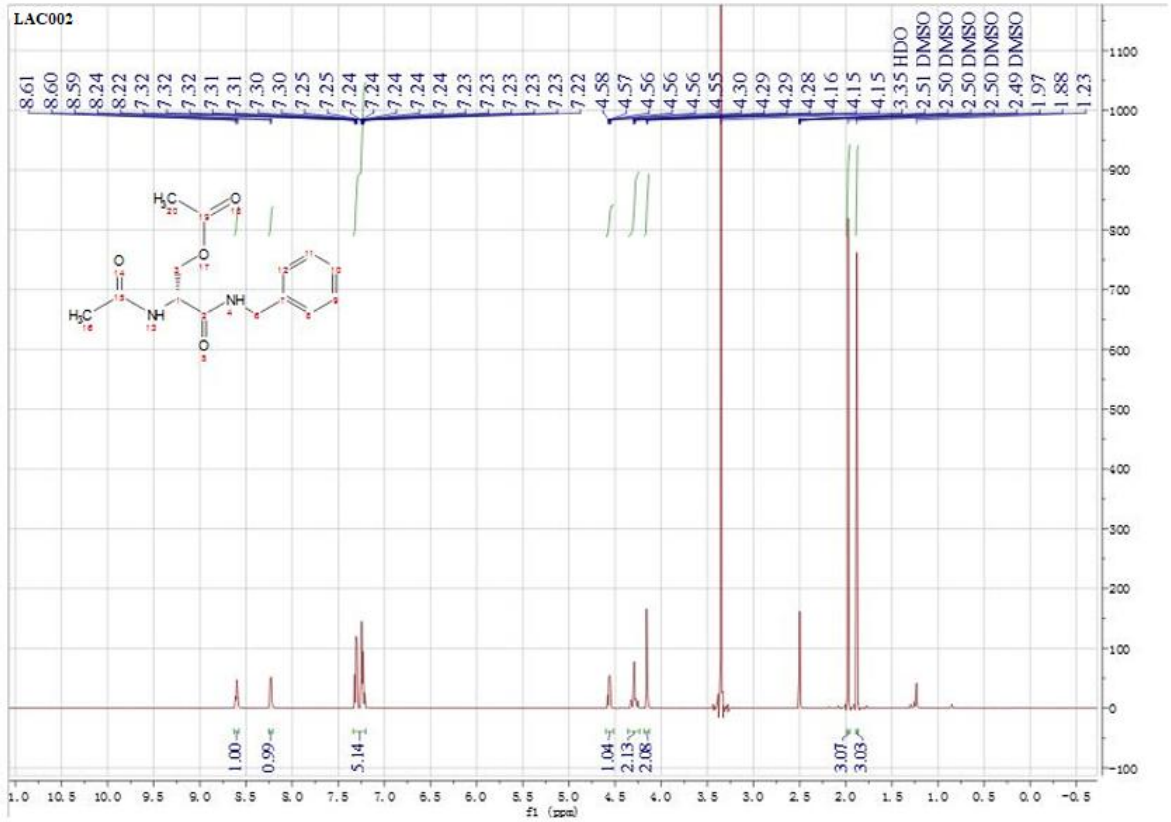


Fig. 15 ^{1}H NMR (600 MHz, DMSO-d6) range of possibilities of LAC002

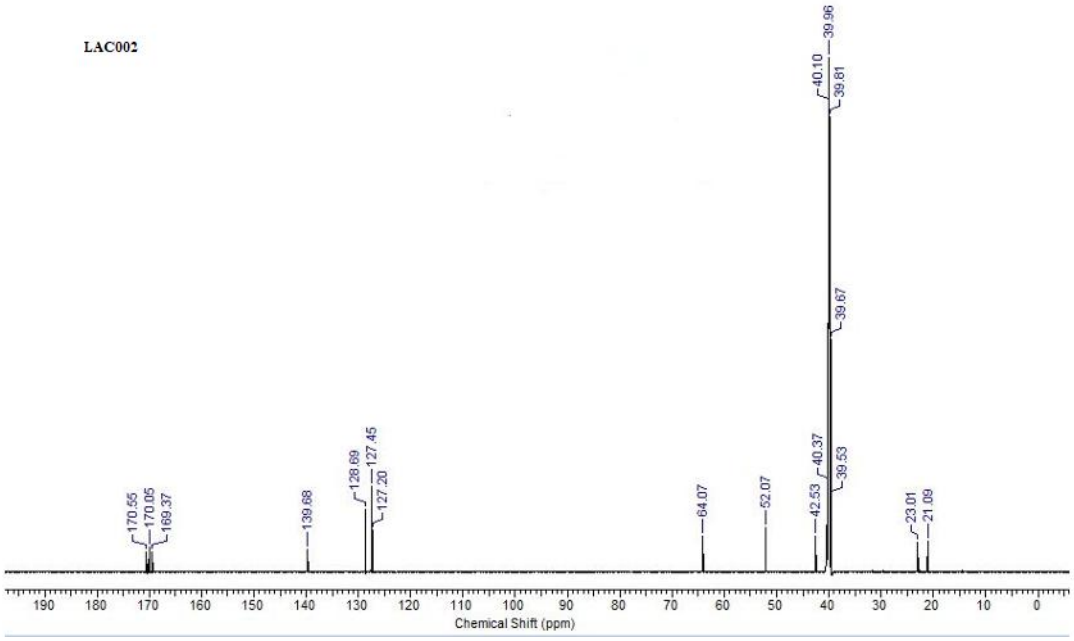


Fig. 16 ^{13}C NMR (100MHz, DMSO-D6) range of possibilities of LAC002

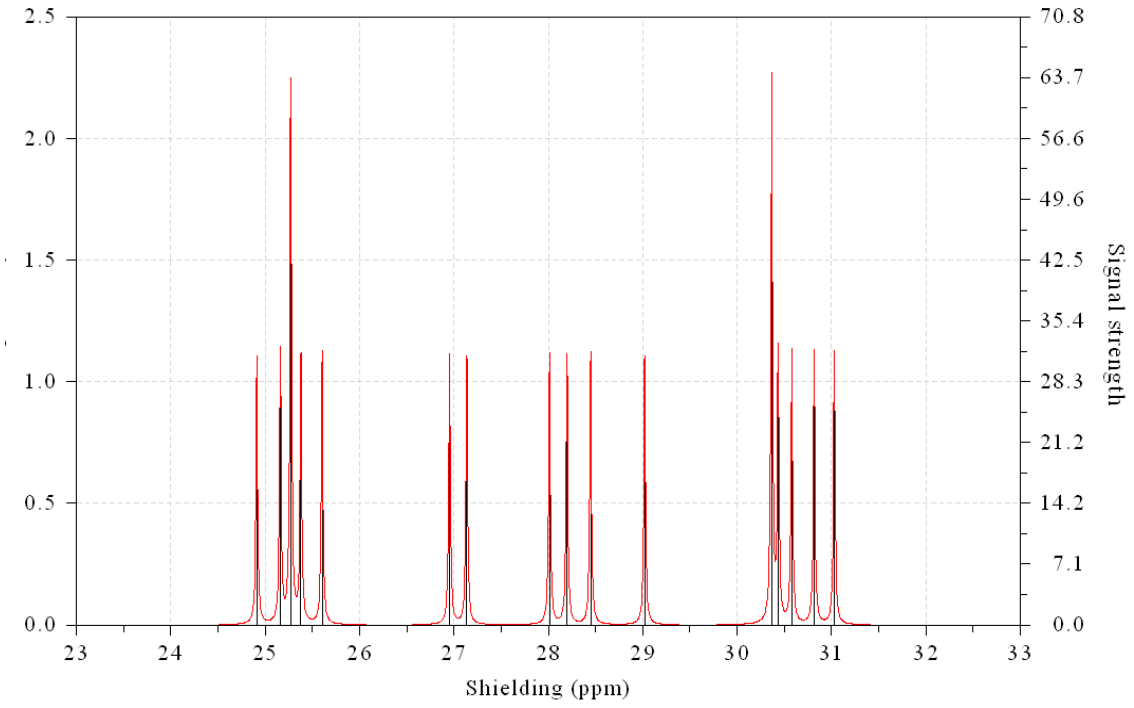


Fig. 17 H NMR computational range of possibilities of LAC002

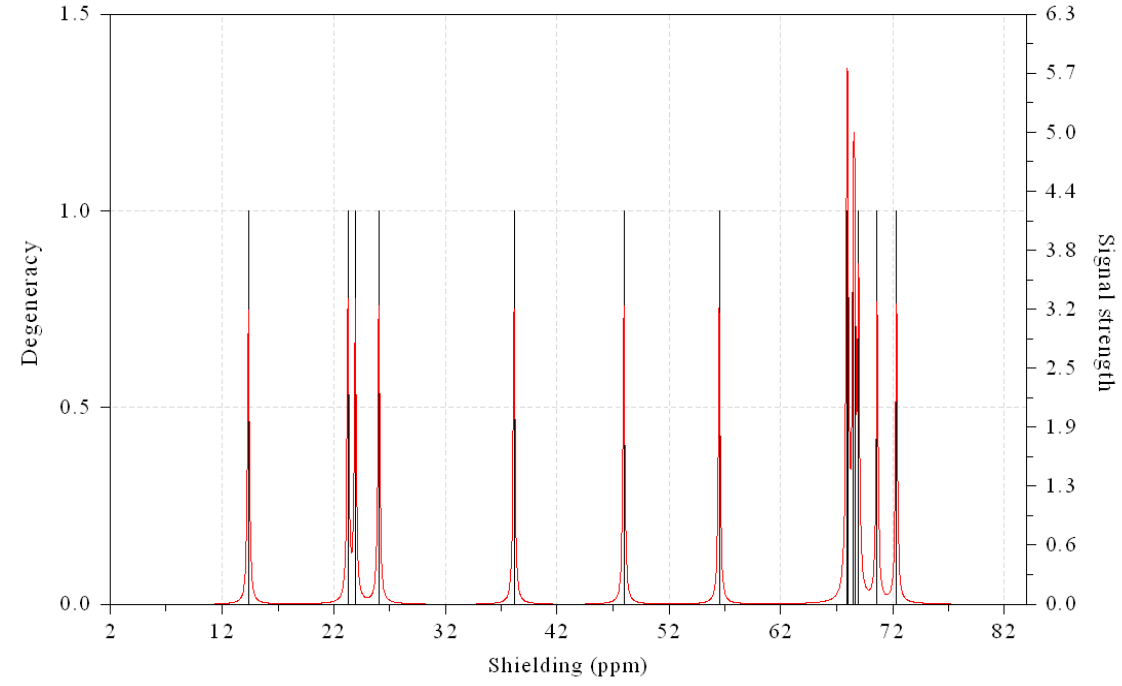


Fig. 18 C NMR computational range of possibilities of LAC002

4.11.1 Studies associated with biology along with pharmaceutical sciences

To find the minimal inhibitory concentration on the Staphylococcus aureus strain, the test item was examined using the microdilution technique. The compounds' MIC on the studied organisms was 10 µg/ml, according to the data.

MATERIALS AND METHODS

1. Incubator- scigenics, India
2. Multimode microplate reader- BioTek, USA
3. Centrifuge- Remi, India
4. *Staphylococcus aureus* (MTCC-96)
5. Resazurin
6. Mueller-Hinton broth from Himedia
7. Spectrophotometer from Eppendorf

METHODOLOGY

Inoculum Preparation and Inoculation

- Using a Mueller-Hinton fermentation plate, isolate the beneficial microbes out of the Glycerol, stocks and incubate it for the whole night at the temperature of 37°C.
- A sterile loop was used to select one colony taken from the experimental plate, and it was subsequently introduced into 10 milliliters of Mueller-Hinton broth medium in a 50 milliliter conical flask. Incubated at 37°C for the whole night while being stirred at 220 rpm.
- Five milliliters of Mueller-Hinton broth medium and 125 microliters of the culture overnight (a 40X dilute solutions of the previous cultures) were placed in an Erlenmeyer container and underwent incubation for two hours at 37°C while being stirred at 220 rpm.
- The concentration of continuously improving inoculation is brought down to around 1X108 CFU/ml.

Preparation of dilutions of Test Compounds

- The test compound is solubilized on DMSO at 10 mg/ml stock.
- From the stock, the working stock is prepared as 4X concentration in Mueller-Hinton broth.
- In the 96-well plate, 50 µl of medium was dispersed to all the wells.
- Then 25 µl of different concentrations of test compound was added to the respective wells.
- In the control wells, 25 µl of plain medium was added.
- From the diluted inoculum suspension, 25 µl was add to each of the wells in column 1 to 10 already containing 75 µl (50µl medium + 25µl test compounds) to yield bacterial concentration of approximately 5 x10^4 CFU/well.
- The time taken to prepare and dispense the OD adjusted bacteria did not exceed 15 min.
- • Following chemical addition to this, the prepared vessel undergoes incubation at 37°C over a period of 24 hours.
- A calculation was made after the coated surface was analyzed on OD 600.
- Following a 24-hour incubation period at 37°C, 30µl of resazurin (0.015%) was transferred to each well. Each of the wells followed by incubation for an additional three hours to see any color changes.

- Colonies that showed no color change (blue resazurin color stayed the same) at the final stage of the period of incubation received the designation for displaying a MIC level exceeding it. Figure 19 shows an appropriate outcome taken from the MIC throughout LAC002.

RESULTS

A representative outcome of the nalidixic acids MIC assessment in S. aerogenosa. When comparison to the background information, the MIC (minimum inhibitory concentration) is the level of concentration at which no noticeable development occurs. The minimum inhibitory concentration (MIC) in this instance was found to be 10 µg/mL. The standard error of a minimum four duplicate measurements is shown by bars that indicate errors. Table 8 shows the LAC002 preliminary values for absorbance at 600 nm on the MIC analysis.

Table:8 Raw Data Absorbance values at 600nm of LAC002 On MIC TEST

Reading at 600 nm

	1	2	3	4	5	6	7	8	9	10	11	12
A	0.108	0.100	0.079	0.072	0.132	0.711	1.055	1.035	1.043	1.059	1.073	0.058
B	0.095	0.096	0.071	0.069	0.179	0.729	1.007	1.046	1.028	1.037	1.033	0.060
C	0.105	0.097	0.081	0.063	0.154	0.639	1.022	1.037	1.042	1.061	1.037	0.052
D	0.098	0.097	0.074	0.075	0.148	0.686	1.048	1.054	1.065	1.013	1.066	0.048

Plate Layout

	1	2	3	4	5	6	7	8	9	10	11	12
A	SPL1:1 100	SPL1:2 50	SPL1:3 25	SPL1:4 10	SPL1:5 5	SPL1:6 2.5	SPL1:7 1	SPL1:8 0.5	SPL1:9 0.1	SPL1:10 0.05	SPLC1 Control	Blank
B	SPL1:1 100	SPL1:2 50	SPL1:3 25	SPL1:4 10	SPL1:5 5	SPL1:6 2.5	SPL1:7 1	SPL1:8 0.5	SPL1:9 0.1	SPL1:10 0.05	SPLC1 Control	Blank
C	SPL1:1 100	SPL1:2 50	SPL1:3 25	SPL1:4 10	SPL1:5 5	SPL1:6 2.5	SPL1:7 1	SPL1:8 0.5	SPL1:9 0.1	SPL1:10 0.05	SPLC1 Control	Blank
D	SPL1:1 100	SPL1:2 50	SPL1:3 25	SPL1:4 10	SPL1:5 5	SPL1:6 2.5	SPL1:7 1	SPL1:8 0.5	SPL1:9 0.1	SPL1:10 0.05	SPLC1 Control	Blank

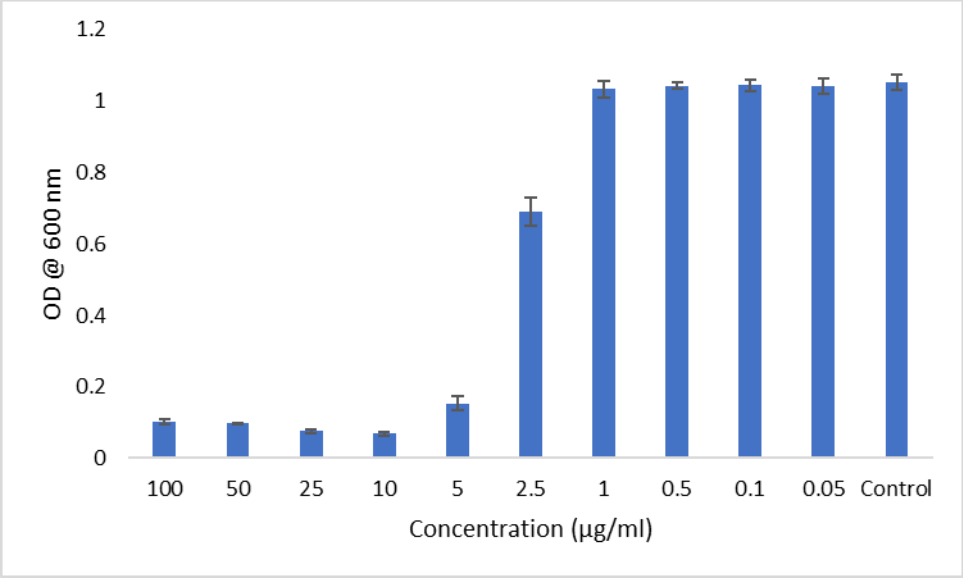


Fig 19. Representative result from the MIC of LAC002

4.11.2 Drug likeness

Early during the process of identifying drugs, drug similarity features are assessed to identify potential matches for subsequent development into an affordable pharmaceutical product.

In the design of drugs, the Lipinski scale out of five is a widely used criterion for evaluating the biological similarity of molecules targeted for consumption orally [52,53]. The rule of five aids in identifying substances that are more likely to exhibit favorable pharmacokinetic characteristics, increasing the likelihood that medication development will be successful. Table 9 shows the estimated values for significant ADME parameters for the LAC002. Considering a TPSA score between 0 and 140 of (Å2), a chemical is more probable to have great bioavailability when consumed since it can greater readily pass through the cell's membrane. It is anticipated that the molecule's molar reactivity would be between 40 and 130. A drug's calculated bioavailability score, which evaluates how rapidly and to what extent it reaches the bloodstream, is 0.55 for LAC002. The lipophilicity characteristics of LAC002 are displayed in Table 9. Lipophilicity is denoting what allows a molecule for dissolving in lipids or fatty substances [54]. This is important for a drug's ability to traverse biological membranes, and partition coefficients are often utilized to measure it.

Table 9: Druglikeness comparison parameters of LAC002.

Properties	LAC002
Rotatable bonds	9
Hydrogen bond acceptors	4
Hydrogen bond donors	2
Molar refractivity	72.35
Topological polar surface area	84.50 ($Å^2$)
Bioavailability score	0.55
Pure water solubility (mg/ml)	5.33
Log kp (cm/s)	-7.78
Lipinski rule violations	0

4.11.3 Molecular docking

Molecular docking is a powerful computational technique that has greatly benefited medical research by evaluating a drug receptor's engagement to enzymes. With this innovative approach, researchers are able to explore the particular interaction regions amongst the substance being studied and proteins [55, 56]. This study contributes to our understanding of how ligands, which are small molecules, move through biological systems. The docking reagent that protein 2GSE requires to target malignant cells must fit into the region where it functions. This protein data library was retrieved from the RCSB website. To determine which interactions might have had been the lowest point the target receptor was placed within each of the numerous classifications of the chosen molecule. The detained adherence with the smallest authorized energy volume was chosen in order to examine the authority plan. The docking characteristics of the chemical with respect to the specific proteins are displayed in Table 10. Gene regulation, immunological response, and signal transmission all depend on protein-ligand interactions. The understanding of biological inhibition mechanisms and the theoretical underpinnings for the development and identification of novel therapeutic targets depend heavily on protein-ligand interactions. To choose the appropriate target protein for docking, the Research Collaboratory for Structural Bioinformatics PDB (RCSB PDB) is used. The title chemical is illustrated using a ligand in Figure 20, showing how it interacts with the proteins 2GSE. The lowest binding energy in this group is - 4.26 kcal/mol for 2GSE, and several of the docked antagonists interacted with the ligand.

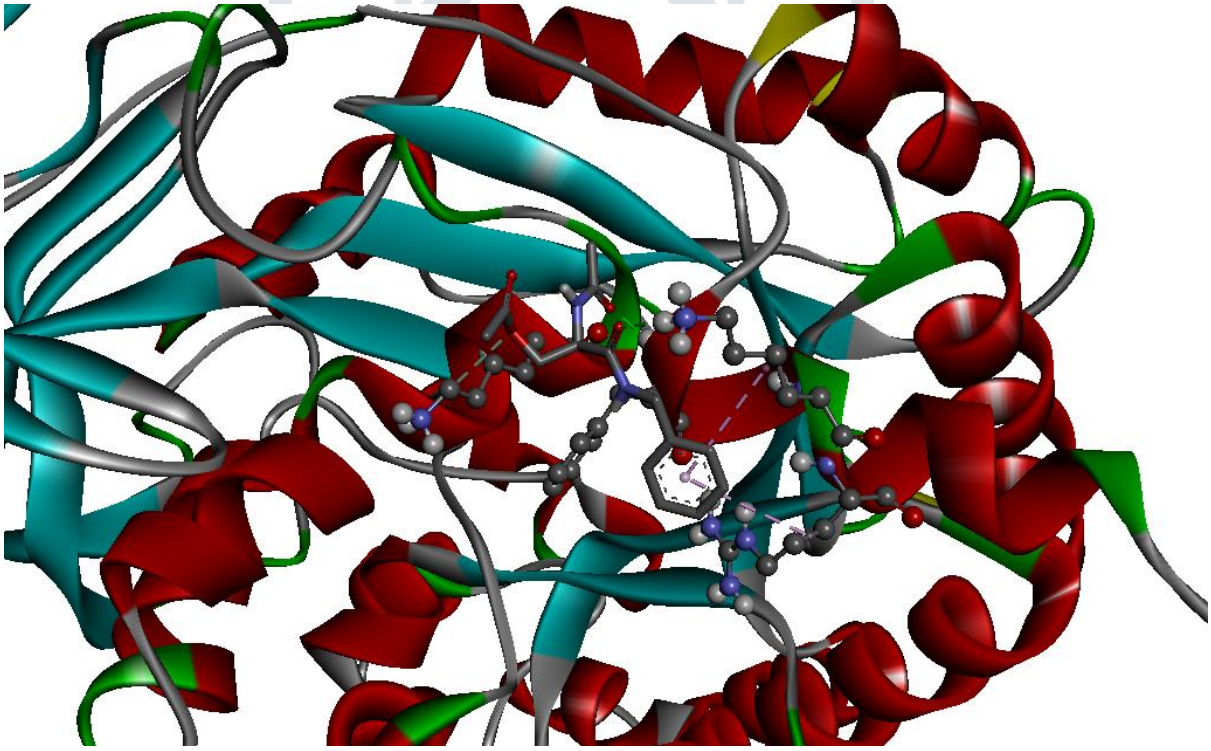


Fig. 20 LAC002 connection with the 2GSE location of interest.

Table 10: LAC002's Molecular Docking outcomes:

S.No.	Compound name	Binding energy Kcal/mol	Inhibition Constant	No. of H-Bonding	Hydrogen bonded amino acids
1.	LAC002	-4.26	7.5 µM	3	PHE474(4.05Å), PRO475 (3.03 Å), 5, ASP4787(3.74 Å), ASP197(3.09 Å), TYR62(3.50 Å)

FUNDING
No Funding is Available for this Research

- **Declaration of interests**

  ➢ The authors declare that they have no known competing financial interests or personal relationships that could have appeared to influence the work reported in this paper.

  ➢ The authors declare the following financial interests/personal relationships which may be considered as potential competing interests: no financial and personal relationships as competing interests.

CREDIT AUTHOR STATEMENT

1. N. ELUMALAI - Writing and Methodology.
2. Dr. MAGESH S- Resources and Data collection
3. Dr. KAMATCHI T- Writing – Review and editing.
4. Dr. C.T. RAVICHANDRAN – Supervision and Validation

5. Conclusion

In the present study, the geometry of the compound LAC002 ([(2*R*)-2-acetamido-3-(benzylamino)-3-oxopropyl] acetate) was optimized using the DFT-B3LYP approach with the 6-311++G(d,p) basis set. The fundamental modes of the optimized geometry's vibrational frequencies and atomic charges have been determined via Mulliken charges of DFT calculations using bond length, bond angle, and other molecular structural data. When assigning wave numbers in the full form based on vibration (PED), the potential energy distribution serves as the foundation. No indication of extra peak forms was found when the synthesized combinations were compared to lacosamide. The C=O peak for LAC002 become more prominent in compositions regarding a considerable proportion of lacosamide (LCM). An extremely good fit between the theoretical Raman and also FTIR frequency ranges was observed. The energy gap between the HOMO and LUMO has been calculated. The MEP analysis shows the locations of the nucleophilic interactions and highly electrophilic attacks. NBO computations were used to study the relationship between bonds of hydrogen production and charge concentration. To ascertain the electronic structure and the absorption band assignments, respectively, DFT calculations and UV spectra for various solvents have been utilized. In contrast to earlier research on lacosamide, LAC002 absorbs UV radiation most effectively at its most intense wavelength of 227 nm. Significant structural modifications are indicated by the 13C NMR spectra for LAC002, and a chemical shift of 1.88 ppm in a 1H NMR spectrum confirms the existence of a proton on a terminal alkyne group (H-C≡C-). The NLO parameters of the title compound signifies its biological activity over optical activity. The MIC biological test and ADME druglikeness of bio active score 0.55 confirms the biological properties of LAC002. The docking result of lowest binding energy of - 4.26 kcal/mol, ligand interaction over protein of anticancer activity shows that the compound LAC002 an anti-epileptic medication serves to target cancerous cell and supress the growth by targeting the active site has been determined. The findings of the study should be useful to just about anyone who is interested in the clinical and theoretical considerations aspects associated with the title molecule being studied.

6. References

[1]. Villanueva, V., J. C. Sanchez-Alvarez, P. Pena, J. Salas-Puig, F. Caballero-Martinez, and A. Gil-Nagel. "Treatment initiation in epilepsy: an expert consensus in Spain." *Epilepsy & Behavior* 19, no. 3 (2010): 332-342. https://doi.org/10.1016/j.yebeh.2010.07.016

[2]. Hauser, W. Allen, John F. Annegers, and Leonard T. Kurland. "Prevalence of epilepsy in Rochester, Minnesota: 1940–1980." *Epilepsia* 32, no. 4 (1991): 429-445. https://doi.org/10.1111/j.1528-1157.1991.tb04675.x

[3]. Berg, Anne T., Shlorao Shinnar, Susan R. Levy, Francine M. Testa, Susan Smith-Rapaport, and Barbara Beckerman. "How well can epilepsy syndromes be identified at diagnosis? A reassessment 2 years after initial diagnosis." *Epilepsia* 41, no. 10 (2000): 1269-1275. https://doi.org/10.1111/j.1528-1157.2000.tb04604.x

[4]. Radhakrishnan, Kurupath. "Challenges in the management of epilepsy in resource-poor countries." *Nature Reviews Neurology* 5, no. 6 (2009): 323-330. https://doi.org/10.1038/nrneurol.2009.53

[5]. Doty, Pamela, G. David Rudd, Thomas Stoehr, and Dirk Thomas. "Lacosamide." *Neurotherapeutics* 4, no. 1 (2007): 145-148. https://doi.org/10.1016/j.nurt.2006.10.002

[6]. Maschio, Marta, Alessia Zarabla, Andrea Maialetti, Alessandra Fabi, Antonello Vidiri, Veronica Villani, and Diana Giannarelli. "Quality of life, mood and seizure control in patients with brain tumor related epilepsy treated with lacosamide as add-on therapy: a prospective explorative study with a historical control group." *Epilepsy & Behavior* 73 (2017): 83-89. https://doi.org/10.1016/j.yebeh.2017.05.031

[7]. Guedes, Isabella A., Leon SC Costa, Karina B. Dos Santos, Ana LM Karl, Gregório K. Rocha, Iury M. Teixeira, Marcelo M. Galheigo et al. "Drug design and repurposing with DockThor-VS web server focusing on SARS-CoV-2 therapeutic targets and their non-synonym variants." *Scientific Reports* 11, no. 1 (2021): 5543.https://doi.org/10.1038/s41598-021-84700-0

[8]. Asif, Mohd, Farrukh Aqil, Fatmah Ali Alasmary, Amani Salem Almalki, Abdul Rahman Khan, and Malik Nasibullah. "Lewis base-catalyzed synthesis of highly functionalized spirooxindole-pyranopyrazoles and their in vitro anticancer studies." *Medicinal Chemistry Research* 32, no. 5 (2023): 1001-1015.https://doi.org/10.1007/S00044-023-03053-7

[9]. de Siqueira, Lucianna Rabelo Pessoa, Paulo André Teixeira de Moraes Gomes, Larissa Pelágia de Lima Ferreira, Moacyr Jesus Barreto de Melo Rêgo, and Ana Cristina Lima Leite. "Multi-target compounds acting in cancer progression: Focus on thiosemicarbazone, thiazole and thiazolidinone analogues." *European Journal of Medicinal Chemistry* 170 (2019): 237-260. https://doi.org/10.1016/j.ejmech.2019.03.024

[10]. Kassem, Asmaa F., Mohamed A. Omar, Eman S. Nossier, Hanem M. Awad, and Wael A. El-Sayed. "Novel pyridine-thiazolidinone-triazole hybrid glycosides targeting EGFR and CDK-2: Design, synthesis, anticancer evaluation, and molecular docking simulation." *Journal of Molecular Structure* 1294 (2023): 136358. https://doi.org/10.1016/j.molstruc.2023.136358

[11]. Anand, G., M. Sivasubramanian, I. Manimehan, A. Ruby, R. Abinayashri, and R. K. Asmitha. "Synthesis, spectroscopic elucidation (FT-IR, FT-Raman, UV–vis), quantum chemical computation (PES, FMO, HOMO–LUMO, MEP, NLO, Hirshfeld) and molecular docking studies on 2-thiophenecarboxamide crystal." *Journal of Molecular Structure* 1286 (2023): 135586. https://doi.org/10.1016/j.molstruc.2023.135586

[12]. Suvitha, A., S. Periandy, S. Boomadevi, and M. Govindarajan. "Vibrational frequency analysis, FT-IR, FT-Raman, ab initio, HF and DFT studies, NBO, HOMO–LUMO and electronic structure calculations on pycolinaldehyde oxime." *Spectrochimica Acta Part A: Molecular and Biomolecular Spectroscopy* 117 (2014): 216-224. https://doi.org/10.1016/j.saa.2013.07.080

[13]. Palabindela, Rambabu, Ramu Guda, Gondru Ramesh, Ramakrishna Bodapati, Satheesh Kumar Nukala, Prabhakar Myadaraveni, Gangalla Ravi, and Mamatha Kasula. "Curcumin based pyrazole-thiazole hybrids as antiproliferative agents: Synthesis, pharmacokinetic, photophysical properties, and docking studies." *Journal of Molecular Structure* 1275 (2023): 134633. https://doi.org/10.1016/j.molstruc.2022.134633

[14]. Yewale, Chetan, Dipesh Baradia, Imran Vhora, Sushilkumar Patil, and Ambikanandan Misra. "Epidermal growth factor receptor targeting in cancer: a review of trends and strategies." *Biomaterials* 34, no. 34 (2013): 8690-8707. https://doi.org/10.1016/j.biomaterials.2013.07.100

[15]. Zhang Z, Zhou L, Xie N, Nice EC, Zhang T, Cui Y, Huang C (2020) Overcoming cancer therapeutic bottleneck by drug repur posing. Signal Transduct Target Ther 2020 51:1–25. https://doi.org/10.1038/s41392-020-00213-8

[16]. Alamri A, Rauf A, Khalil AA, Alghamdi A, Alafnan A, Als hammari A, Alshammari F, Malik JA, Anwar S (2021) In Silico Screening of Marine Compounds as an Emerging and Promising Approach against Estrogen receptor alpha-positive breast Cancer. Biomed Res Int 2021:1–7. https://doi.org/10.1155/2021/9734279

[17]. Malik JA, Ahmed S, Momin SS, Shaikh S, Alafnan A, Alanazi J, Hajaj M, Almermesh S, Anwar S (2022) Drug Repurposing: a New Hope in Drug Discovery for prostate Cancer. ACS Omega. https://doi.org/10.1021/acsomega.2c05821

[18]. Anwar S, Malik JA, Ahmed S, Kameshwar VA, Alanazi J, Alamri A, Ahemad N (2022) Can Natural Products Targeting EMT serve as the future Anticancer therapeutics? Mol 2022 27:7668. https://doi.org/10.3390/MOLECULES27227668

[19]. Aroosa, Mir, Jonaid Ahmad Malik, Sakeel Ahmed, Onur Bender, Nafees Ahemad, and Sirajudheen Anwar. "The evidence for repurposing anti-epileptic drugs to target cancer." *Molecular Biology Reports* 50, no. 9 (2023): 7667-7680. https://doi.org/10.1007/s11033-023-08568-1

[20]. Medimagh, Mouna, Noureddine Issaoui, Sofian Gatfaoui, Omar Al-Dossary, Aleksandr S. Kazachenko, Houda Marouani, and Marek J. Wojcik. "Molecular modeling and biological activity analysis of new organic-inorganic hybrid: 2-(3, 4-dihydroxyphenyl) ethanaminium nitrate." *Journal of King Saud University-Science* 33, no. 8 (2021): 101616. https://doi.org/10.1016/j.jksus.2021.101616

[21]. Noureddine, Olfa, Noureddine Issaoui, Sofian Gatfaoui, Omar Al-Dossary, and Houda Marouani. "Quantum chemical calculations, spectroscopic properties and molecular docking studies of a novel piperazine derivative." *Journal of King Saud University-Science* 33, no. 2 (2021): 101283. https://doi.org/10.1016/j.jksus.2020.101283

[22]. G.A. Zhurko, D.A. Zhurko, Chemcraft Program, Academic version 1.5, 2004.

[23]. Glendening, E. D., A. E. Reed, J. E. Carpenter, and F. Weinhold. "NBO Version 3.1. Gaussian Inc., Pittsburgh." *References-Scientific Research Publishing nd* (2003).

[24]. De Graef, Marc, and Michael E. McHenry. *Structure of materials: an introduction to crystallography, diffraction and symmetry*. Cambridge University Press, 2012.

[25]. Malagoli, M., and J. L. Brédas. "Density functional theory study of the geometric structure and energetics of triphenylamine-based hole-transporting molecules." *Chemical Physics Letters* 327, no. 1-2 (2000): 13-17. https://doi.org/10.1016/S0009-2614(00)00757-0

[26]. P. Shafieyoon, E. Mehdipour, and Y. S. Mary, "Synthesis, characterization and biological investigation of glycine-based sulfonamide derivative and its complex: Vibration assignment, HOMO – LUMO analysis, MEP and molecular docking," J. Mol. Struct., vol. 1181, pp. 244–252, Apr. 2019, doi:10.1016/j.molstruc.2018.12.067.

[27]. S. Selvakumari, C. Venkataraju, S. Muthu, P. Sangeetha, R. Rajesh, Vibrational spectroscopic, electronic influences, reactivity analysis and molecular docking studies of 2-Fluoro-4-iodo-5-methylpyridine, J. Spectrosc. Lett. (2022) 14–24, https://doi.org/10.1080/00387010.2022.2160462.

[28]. R. Hoffmann, Solids and Surfaces: A Chemist's View of Bonding in Extended Structures, VCH Publishers, New York, 1988.

[29]. J.G. Małecki, Polyhedron 29 (2010) 2157–2165.

[30]. N.M. O'Boyle, A.L .& Tenderholt, K.M. Langner, J Comput Chem 29 (2008) 839–845.

[31]. P. Shafieyoon, E. Mehdipour, and Y. S. Mary, "Synthesis, characterization and biological investigation of glycine-based sulfonamide derivative and its complex: Vibration assignment, HOMO – LUMO analysis, MEP and molecular docking," J. Mol. Struct., vol. 1181, pp. 244–252, Apr. 2019, doi: 10.1016/j.molstruc.2018.12.067.

[32]. R. Mathammal, K. Sangeetha, M. Sangeetha, R. Mekala, S. Gadheeja, Molecular structure, vibrational, UV, NMR, HOMO-LUMO, MEP, NLO, NBO analysis of 3, 5 di tert butyl 4 hydroxybenzoic acid, J. Mol. Struct. 1120 (2016) 1–14.

[33]. B. Fathima Rizwana, J.C. Prasana, S. Muthu, C.S. Abraham., Comput. Biol. Chem. 78 (2019) 9–17

[34]. H. Jacobsen, Can. J. Chem. 86 (2008) 695–702.

[35]. N. Issaoui, H. Ghalla, S.A. Brandan, F. Bardak, H.T. Flakus, A. Atac, B. Oujia, J. Mol. Struct. 1135 (2017) 209–221.

[36]. I. Csizmadia, Theory and practice of mo calculations on organic molecules, Elsevier, 2016, June 23.

[37]. M. Tamer, H. Mahmoody, K.F. Feyzioˇ glu, O. Kılınç, D. Avci, O. Orun, N. Dege, Y. Atalay, Synthesis of the first mixed ligand Mn (II) and Cd (II) complexes of 4- methoxy-pyridine-2-carboxylic acid, molecular docking studies and investigation of their anti-tumor effects in vitro, Appl. Organomet. Chem. 34 (3) (2019, December 23), https://doi.org/10.1002/aoc.5416.

[38]. N. Elangovan, S.Y. Alomar, S. Sowrirajan, B. Rajeswari, A. Nawaz, A.N. Kalanthoden, Photoluminescence property and solvation studies on (E)-N-(pyrimidin2yl)-4-((3,4,5-trimethoxy benzylidede) amino) benzene sulfonamide; Synthesis, structural, topological analysis, antimicrobial activity and molecular docking studies, Inorg. Chem. Commun. 155 (2023) 111019, https://doi.org/10.1016/j.inoche.2023.111019.

[39]. I. Csizmadia, Theory and practice of mo calculations on organic molecules, Elsevier, 2016, June 23.

[40]. M. Tamer, H. Mahmoody, K.F. Feyzioˇ glu, O. Kılınç, D. Avci, O. Orun, N. Dege, Y. Atalay, Synthesis of the first mixed ligand Mn (II) and Cd (II) complexes of 4- methoxy-pyridine-2-carboxylic acid, molecular docking studies and investigation of their anti-tumor effects in vitro, Appl. Organomet. Chem. 34 (3) (2019, December 23), https://doi.org/10.1002/aoc.5416.

[41]. Han, Chang-Soo, Seungsu Kim, Dong-Won Oh, Jeong Yeol Yoon, Eun-Seok Park, Yun-Seok Rhee, Ju-Young Kim, Dae Hwan Shin, Dong-Wook Kim, and Chun-Woong Park. "Preparation, characterization, and stability evaluation of taste-masking Lacosamide microparticles." *Materials* 12, no. 6 (2019): 1000.

[42]. Allegaert S. Ph.D. Thesis. University College Cork; Cork City, Ireland: 2016. Study of the Relation between the Shape of Lacosamide Crystals and the Composition of Crystallization Medium.

[43]. Apexa, Patel, Suhagia Bhanubhai, Parikh Bhumi, Shah Arpan, and Patwari Arpit. "EXTRACTIVE SPECTROPHOTOMETRIC METHOD FOR DETERMINATION OF LACOSAMIDE IN BULK AND ITS PHARMACEUTICAL DOSAGE FORM." (2014).

[44]. Kommineni Lahari, K. Pravallika, K. Lakshmi sai Mounika, M. Bhavya, CH. Dileep kumar, J. Karunakar, & P. Srinivasa babu. (2020). Development of a novel UV spectrophotometric method for the estimation of lacosamide in both bulk and solid dosage forms. *International Journal of Pharmacy and Analytical Research*, *9*(4), 237–242. https://doi.org/10.61096/ijpar.v9.iss4.2020.237-242

[45]. Gobalakrishnan, P., Muni Sekhar Vonteru, Hemanth Kumar, and G. Sadik. "Development and Validation of new analytical methods for the estimation of Lacosamide by UV Spectroscopy." *Asian Journal of Chemical and Pharmaceutical Research* 12, no. 1 (2024): 06-09.

[46]. J.S.P.P. leela , R. Hemamalini , S. Muthu , A .A . Al-Saadi , Spectrochim. Acta Part A 146 (2015) 177–186 .

[47]. N. Swarnalatha , S. Gunasekaran , S. Muthu , M. Nagarajan , Spectrochim. Acta Part A 137 (2015) 721–729 .

[48]. S. Gunasekaran , S. Seshadri , S. Muthu , S. Kumaresan , R. Arunbalaji , Spectrochim. Acta Part A 70 (2008) 550–556 .

[49]. Balci, M. "12—Chemical shift." *Basic 1H-and 13C-NMR spectroscopy. Elsevier Science, Amsterdam* (2005): 283-292.

[50]. Ramisetti, Nageswara Rao, Ramakrishna Kuntamukkala, Sridhar Lakshetti, and Prabhakar Sripadi. "Identification and characterization of stress degradants of lacosamide by LC–MS and ESI-Q-TOF-MS/MS: development and validation of a stability indicating RP-HPLC method." *Journal of Pharmaceutical and Biomedical Analysis* 95 (2014): 256-264.

[51]. Zhou, Na, Tao Li, Lianfeng Ai, Chunhai Guo, Juan Zhang, Shan Fu, and Qiao Wang. "Identification of forced degradation products of lacosamide by LC-QQLIT-MS and LC-IT/TOF-MS." *Acta Chromatographica* 31, no. 1 (2019): 12-18.

[52]. B. Sathya, S. Karthi, K. Ajaijawahar, M. Prasath, Probing the vibrational spectroscopic properties and binding mechanism of anti-influenza agent liquiritin using experimental and computational studies, Res. Chem. Intermed. 46 (2020) 4475–4507, https://doi.org/10.1007/s11164-020-04216-6.

[53]. V. Vetrivelan, Spectra, electronic properties, biological activities and Molecular docking investigation on sulfonamide derivative compound: an Experimental and computational approach, J. Nanosci. Technol. 04 (2018) 348–352, https://doi.org/ 10.30799/jnst.sp203.18040203.

[54]. I. Moriguchi, S. Hirono, I. Nakagome, H. Hirano, Comparison of reliability of log P values for drugs calculated by several methods, Chem. Pharm. Bull. (tokyo) 42 (1994) 976–978, https://doi.org/10.1248/cpb.42.976.

[55]. K. Parveen Begaum, T. Prabhu, M. Thirunavukkarasu, P. Sangeetha, S. Javed, J. M. Khaled, G. Abbas, S. Muthu, J. Chem. Phys. Impact (2023), https://doi.org/ 10.1016/j.chphi.2023.100272.

[56]. I. Jomaa, N. Issaoui, Thierry Roisnel & Houda Marouani, J. Iran. Chem. Soc. 19 (2022) 2527–2542.